

UNIVERSITÀ DEGLI STUDI DI NAPOLI "FEDERICO II"  
FACOLTÀ DI MEDICINA E CHIRURGIA



DOTTORATO IN NEUROSCIENZE  
XXI CICLO

**TESI DI DOTTORATO:**

*ROLE OF THE  $K^+$ -DEPENDENT  $Na^+/Ca^{2+}$  EXCHANGER  
ISOFORM 2 (NCKX2) IN THE DEVELOPMENT OF  
FOCAL CEREBRAL ISCHEMIA*

COORDINATORE:  
CH.MO PROF LUCIO ANNUNZIATO

TUTORE:  
CH.MO PROF LUCIO ANNUNZIATO

CANDIDATO:  
DOTT.SSA ROSARIA GALA

ANNO ACCADEMICO 2007-2008

# INDEX

PREMISES.....	0
INTRODUCTION.....	3
CEREBRAL ISCHEMIA .....	3
<i>Metabolic disruption during ischemia</i> .....	3
<i>Glutamate release</i> .....	4
<i>Focal versus global ischemia.</i> .....	5
NA <sup>+</sup> AND CA <sup>2+</sup> TRANSPORTERS.....	7
<i>Na<sup>+</sup>/Ca<sup>2+</sup> Exchangers</i> .....	9
<i>NCX and NCKX</i> .....	10
<i>NCKX</i> .....	12
<i>Cloning and Tissue Distribution of the five NCKX Isoforms</i> .....	12
<i>NCKX in the Brain</i> .....	14
<i>Ion selectivity and apparent dissociation constants</i> .....	20
<i>Pharmacology of NCKX</i> .....	22
AIM OF THE STUDY.....	24
MATERIALS AND METHODS.....	25
<i>Experimental groups</i> .....	25
<i>Surgical procedures</i> .....	25
<i>Monitoring of arterial blood pressure, CBF, and blood gas concentration.</i> .....	27
<i>Cerebrovascular anatomy evaluation of nckx2<sup>+/+</sup> and nckx2<sup>-/-</sup> mice.</i> .....	28
<i>RNA expression analysis by real-time PCR</i> .....	30
<i>Western blot analysis</i> .....	30
<i>In situ hybridization</i> .....	31
<i>Autoradiography.</i> .....	33
<i>Image analysis</i> .....	33
<i>Data processing</i> .....	33
<i>NeuN immunohistochemistry</i> .....	34
<i>Antisense oligodeoxynucleotide design</i> .....	35
<i>Evaluation of AS-ODN efficacy in vitro and in vivo</i> .....	36

<i>Evaluation of the ischemic volume in rats treated with AS-ODN...</i>	36
<i>Evaluation of the ischemic volume and neurological deficits in</i>	
<i>nckx2+/+ C57BL/6 wild-type mice and nckx2-/- mice.....</i>	37
<i>Primary cortical neurons.....</i>	37
<i>[Ca<sup>2+</sup>]<sub>i</sub> measurement.....</i>	38
<i>Electrophysiology.....</i>	39
<i>Statistical analysis.....</i>	41
RESULTS.....	42
TIME COURSE OF NCKX2 MRNA EXPRESSION BY REAL-TIME PCR IN THE ISCHEMIC CORE AND IN THE AREA SURROUNDING THE ISCHEMIC CORE AFTER PMCAO IN RATS .....	42
NCKX2 MRNA EXPRESSION IN THE PREFRONTAL CORTEX, CINGULATE, MOTOR AND SOMATOSENSORY CORTICES, AND CAUDATE–PUTAMEN OF SHAM-OPERATED AND PMCAO-BEARING RATS EVALUATED 24 H AFTER PMCAO .....	43
TIME COURSE OF NCKX2 PROTEIN EXPRESSION EVALUATED BY WESTERN BLOT IN THE ISCHEMIC CORE AND IN THE REMAINING IPSILATERAL NONISCHEMIC AREA AFTER PMCAO IN RATS.....	47
EFFECT OF NCKX2 KNOCK-DOWN BY ANTISENSE STRATEGY ON THE INFARCT VOLUME INDUCED BY PMCAO IN RATS .....	48
EFFECT OF NCKK2 KNOCK-OUT ON INFARCT VOLUME AND ON NEUROLOGICAL SCORES INDUCED BY TMCAO IN NCKX2+/+ AND NCKX2-/- MICE .....	49
EFFECT OF NCKX2 KNOCK-OUT ON [Ca <sup>2+</sup> ] <sub>i</sub> IN CORTICAL NEURONS EXPOSED TO OGD FOLLOWED BY REOXYGENATION .....	52
EFFECT OF NCKX2 GENETIC ABLATION ON CELL SURVIVAL IN PRIMARY CORTICAL NEURONS EXPOSED TO OGD FOLLOWED BY REOXYGENATION...	53
EFFECT OF NCKX2 KNOCK-OUT ON INCKX IN THE FORWARD AND REVERSE MODES OF OPERATION IN PRIMARY CORTICAL NEURONS .....	54
CONCLUSION AND DISCUSSION.....	57
REFERENCES.....	61

# PREMISES

Hypoxic-ischemic brain injury continues to be the third leading cause of death in the western world, affecting millions of victims each year. Of these, nearly one-third will die and another third will be left with severe and permanent disability. In 2005, almost 6 millions people died because of cerebral ischemia, in the world.

The brain is the internal organ that functions with the greatest expenditure of metabolic energy. Among the various internal organs that constitute the human body, the central nervous system is unique in the sense that the energy metabolism of neurons almost completely depends on aerobic glycolysis. Hence, cerebral infarction, which occurs because of an insufficient or obstructed blood supply, leads to the immediate failure of brain nutrition and oxygenation. Furthermore, in accordance with the aging of the population in many advanced countries, the incidence of this disease is currently growing rapidly (Ogawa et al.)

Unlike ischemic injury to many other tissues, the severity of disability is not well predicted by the amount of brain tissue lost. For example, damage to a small area in the medial temporal lobe may lead to severe disability, such as loss of speech, while damage to a greater volume elsewhere has little effect on function. The degree of disability does not simply

reflect the severity or distribution of impaired blood supply. Populations of cells lying side by side in the brain can display dramatically different vulnerabilities to equivalent degrees of ischemia. Although a great deal has been learned about how nervous system anatomy, physiology and biochemistry interact to modify hypoxic-ischemic brain injury, much remains to be learned about what features contribute to the special vulnerability of the brain to stroke and of specific cell populations to hypoxic-ischemic injury during stroke (Siegel et al., 1999).

# INTRODUCTION

## CEREBRAL ISCHEMIA

### ***Metabolic disruption during ischemia***

Normal energy metabolism in the brain has several unusual features, including a high metabolic rate, limited intrinsic energy stores and critical dependence on aerobic metabolism of glucose. Reflecting this special metabolic status, as well as the existence of several unique injury mechanisms discussed below, the brain exhibits higher vulnerability to ischemic injury than most other tissues. Ischemic brain injury occurs in several clinical settings. The most common is *stroke*, focal disruption of blood supply to a part of the brain. Other settings include transient impairment of blood flow to the entire brain, *global ischemia*, as occurs during cardiac arrest.

When brain hypoxia or ischemia occurs, tissue energy demands cannot be met, so ATP levels fall. Loss of ATP results in decreased function of active ion pumps, such as the Na/K-ATPase, the most important transporter for maintaining high intracellular concentrations of K<sup>+</sup> (~155 mM) and low intracellular concentrations of Na<sup>+</sup> (~12 mM). Loss of ion pump function allows rundown of transmembrane ion gradients, leading to membrane depolarization, the opening of voltage-sensitive ion channels and a cascade of subsequent events,

which, if sustained, lead ultimately to cell death. Depending on the circumstances, this death may be restricted to selectively vulnerable neuronal populations or may involve all cells (tissue infarction).

Within seconds of an ischemic insult, normal brain electrical activity ceases due to the activation of membrane  $K^+$  channels and widespread neuronal hyperpolarization (Kristian and Siesjo, 1997). The hyperpolarization, presumably protective, however fails to preserve high-energy phosphate levels in tissue as concentrations of phosphocreatine (PCr) and ATP fall within minutes after ischemia onset (Welch et al, 1997). The fall in  $pO_2$  during ischemia leads to enhanced lactic acid production as cells undergo a Pasteur shift from a dependence on aerobic metabolism to a dependence on glycolysis. The resulting lactic acidosis decreases the pH of the ischemic tissue from the normal 7.3 to intra-ischemic values ranging from 6.8 to 6.2. In addition, efflux of  $K^+$  from depolarizing neurons results in prolonged elevations in extracellular  $[K^+]$  and massive cellular depolarization, a state known as *spreading depression*, which can propagate in the brain tissue. Rapid inactivation of  $O_2$ -sensitive  $K^+$  channels by decreased  $pO_2$  may represent one mechanism whereby neurons put a brake on this ongoing  $K^+$  efflux (Haddad and Jiang, 1997) . Other cellular ion gradients are also lost; thus, intracellular  $Na^+$  and  $Ca^{2+}$  rise and intracellular  $Mg^{2+}$  falls (Siegel et al., 1999).

### ***Glutamate release***

Extracellular concentrations of many neurotransmitters are increased during hypoxia-ischemia. Depolarization-induced

entry of  $\text{Ca}^{2+}$  via voltage-sensitive  $\text{Ca}^{2+}$  channels stimulates release of vesicular neurotransmitter pools, including the excitatory amino acid neurotransmitter glutamate. At the same time,  $\text{Na}^+$ -dependent uptake of certain neurotransmitters, including glutamate, is impaired. High-capacity uptake of glutamate by the glutamate transporter couples the uptake of one glutamate and two  $\text{Na}^+$  with the export of one  $\text{K}^+$  and one  $\text{HCO}_3^-$  (or  $\text{OH}^-$ ). When the cellular ion gradients are discharged, the driving force for glutamate uptake is lost. In addition, glutamate uptake by the widely expressed astrocyte high-affinity glutamate transporter GLT-1, or excitatory amino acid transporter-2 (EAAT2), and the neuronal transporter, or EAAT3, can be downregulated by free radical-mediated oxidation of a redox site on the transporter (Trotti et al., 1997). Furthermore, since the transporter is electrogenic, that is, normally transferring a positive charge inward, membrane depolarization can lead to reversal of the transporter, producing glutamate efflux (Nicholls and D. Attwell, 1990). Thus, both impaired glutamate uptake and enhanced glutamate release contribute to sustained elevations of extracellular glutamate in the ischemic brain. Microdialysis of ischemic rat brain has detected an increase from the resting extracellular glutamate concentrations of 1 to 2  $\mu\text{M}$  up to concentrations in the high micromolar or even low millimolar range.

### ***Focal versus global ischemia.***

Ischemic injury to the brain can result from several different processes. Focal ischemia, which accounts for a majority of strokes, occurs when an artery supplying a region of the brain

is occluded, either by an embolus, which is generally material broken off from a plaque in a large artery or a thrombus in the heart, or by a thrombus or platelet plug which forms directly in the affected artery. While focal ischemic insults generally reflect the distribution of vascular supply to a region, the area of infarction is typically less than the entire distribution of the occluded artery due to the presence of collateral circulation at the borders of the region supplied by the occluded vessel. The ultimate area of infarction will depend on the duration and degree of vascular occlusion and the availability of collateral blood supply (Graham and Brierly, 1984) . The region of the brain supplied uniquely by the occluded artery develops the most severe injury, termed the *ischemic core*, while the rim of tissue surrounding the core, termed the *penumbra*, which has the benefit of some maintained blood flow supplied by collateral circulation, sustains less severe injury. Focal ischemia may also accompany other acute brain insults, such as intracerebral hemorrhage or trauma.

Reversible global ischemia, such as occurs during cardiac arrest and resuscitation, reflects a transient loss of blood flow to the entire brain and generally results in the death of certain selectively vulnerable neuronal populations. Hypoxia accompanies ischemic insults but may also occur without loss of blood flow, for example, during near drowning or carbon monoxide poisoning. Hypoglycemia produces brain injury that has several features in common with ischemic injury. Neurons are more susceptible than glial cells to ischemia, hypoxia or hypoglycemia; and the phylogenetically newer regions of the brain, including the cortex and cerebellum, are affected to a

greater extent than the brainstem (Graham and Brierly, 1984). Several other cell types, such as astrocytes, oligodendroglia, and endothelial cells, show a phenotype that is more resistant to ischemic conditions, compared to neurons (Siesjö BK, 1988). Anyway the selective vulnerability of certain neurons cannot be explained by simply considering the vascular distribution (Vogt and Vogt, 1984): the juxtaposition of relatively vulnerable and relatively resistant neuronal populations within a single vascular distribution suggests that intrinsic tissue factors contribute heavily to ischemic neuronal vulnerability. For example, pyramidal neurons in the CA1 subfield of the hippocampus die after 5 to 10 min of global ischemia, while neurons in the nearby CA3 region are preserved. Populations of neurons that are selectively vulnerable to ischemia include cortical pyramidal neurons, cerebellar Purkinje cells, hippocampal CA1 pyramidal neurons and subpopulations in the amygdala, striatum, thalamus and brainstem nuclei.

## **Na<sup>+</sup> AND Ca<sup>2+</sup> TRANSPORTERS**

The discussion of the molecular basis of electrical signaling takes for granted the fact that nerve cells maintain ion concentration gradients across their surface membranes. However, none of the ions of physiological importance (Na<sup>+</sup>, K<sup>+</sup>, Cl<sup>-</sup>, and Ca<sup>2+</sup>) are in electrochemical equilibrium. Because channels produce electrical effects by allowing one or more of these ions to diffuse down their electrochemical gradients, there would be a gradual dissipation of these concentration

gradients unless nerve cells could restore ions displaced during the current flow that occurs as a result of both neural signaling and the continual ionic leakage that occurs at rest. The work of generating and maintaining ionic concentration gradients for particular ions is carried out by a group of plasma membrane proteins known as **active transporters** (Purves et al., 2001).

Several types of active transporter have now been identified. Although the specific jobs of these transporters differ, all must translocate ions against their electrochemical gradients. Moving ions uphill requires the consumption of energy, and neuronal transporters fall into two classes based on their energy sources. Some transporters acquire energy directly from the hydrolysis of ATP and are called ATPase pumps. The most prominent example of an ATPase pump is the  $\text{Na}^+/\text{K}^+$  ATPase pump, which is responsible for maintaining transmembrane concentration gradients for both  $\text{Na}^+$  and  $\text{K}^+$ . Another is the  $\text{Ca}^{2+}$  ATPase pump, which provides one of the main mechanisms for removing  $\text{Ca}^{2+}$  from cells. The second class of active transporter does not use ATP directly, but depends instead on the electrochemical gradients of other ions as an energy source. This type of transporter carries one or more ions *up* its electrochemical gradient while simultaneously taking another ion (most often  $\text{Na}^+$ ) *down* its gradient. Because at least two species of ions are involved in such transactions, these transporters are usually called ion exchangers.

An example of such a transporter is the  $\text{Na}^+/\text{Ca}^{2+}$  exchanger, which shares with the  $\text{Ca}^{2+}$  pump the important job of keeping intracellular  $\text{Ca}^{2+}$  concentrations low (Purves et al., 2001).

### ***Na<sup>+</sup>/Ca<sup>2+</sup> Exchangers***

The  $\text{Na}^+/\text{Ca}^{2+}$  exchanger belongs to the superfamily of membrane proteins (Fig.1) comprising the following members (Annunziato et al., 2004):

1) the NCX family, which exchanges three  $\text{Na}^+$  ions for one  $\text{Ca}^{2+}$  ion or four  $\text{Na}^+$  ions for one  $\text{Ca}^{2+}$  ion depending on  $[\text{Na}^+]_i$  and  $[\text{Ca}^{2+}]_i$  (Reeves and Hale, 1984; Fujioka et al., 2000; Hang and Hilgemann, 2004);

2) the NCKX ( $\text{Na}^+/\text{Ca}^{2+}$  exchanger  $\text{K}^+$ -dependent) family, which exchanges four  $\text{Na}^+$  ions for one  $\text{Ca}^{2+}$  plus one  $\text{K}^+$  ion (Schnetkamp et al., 1989; Lytton et al., 2002);

3) the bacterial family which probably promotes  $\text{Ca}^{2+}/\text{H}^+$  exchange (Cunningham and Fink, 1996);

4) the nonbacterial  $\text{Ca}^{2+}/\text{H}^+$  exchange family, which is also the  $\text{Ca}^{2+}$  exchanger of yeast vacuoles (Pozos et al., 1996);

5) the  $\text{Mg}^{2+}/\text{H}^+$  exchanger, an electrogenic exchanger of protons with  $\text{Mg}^{2+}$  and  $\text{Zn}^{2+}$  ions (Shaul et al., 1999). These membrane proteins are all peculiarly characterized by the presence of  $\alpha$ -repeats, the regions involved in ion translocation.



accessibility from the extracellular environment to the cytosol and vice versa. Unlike ion channels, each ion translocation event of the NCX and NCKX proteins is thought to be accompanied by a major conformational change, and these proteins are therefore thought to exist in at least two, and possibly more distinct conformational states (Altimimi and Schnetkamp, 2007). Perhaps the best evidence for the alternating access model in the case of the NCX and NCKX proteins is the well-established occurrence of self-exchange fluxes in both NCKX,  $(Ca^{2+}+K^+):(Ca^{2+}+K^+)$ , (Schnetkamp PPM, 1980; Schnetkamp et al., 1991a) and NCX,  $Ca^{2+}:Ca^{2+}$ , (Philipson and Nishimoto, 1981) at rates comparable to  $Na^+/Ca^{2+}(+K^+)$  exchange fluxes. Another important physiological consequence of the alternating access model is that NCX and NCKX proteins are expected to be bidirectional. NCX and NCKX proteins can mediate both  $Ca^{2+}$  extrusion (forward exchange) as well as  $Ca^{2+}$  import (reverse exchange), dependent on the transmembrane  $Na^+$  gradient and to a lesser degree on membrane potential and on the transmembrane  $K^+$  gradient (NCKX only) (Schnetkamp PPM, 1989; Reeves JP, 1985).

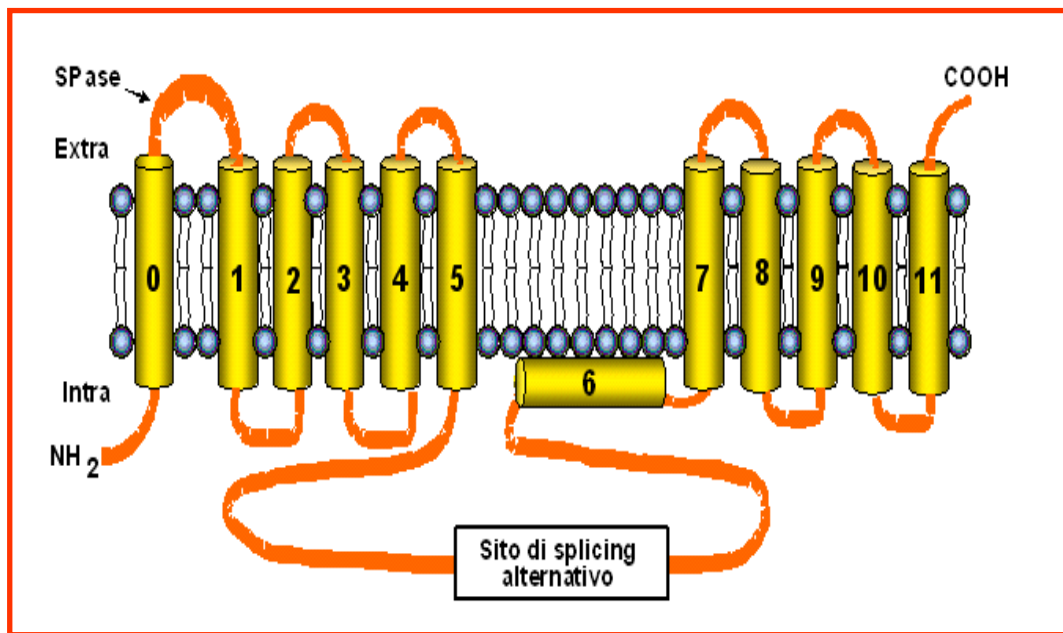


**Fig. 2** Topological Model of NCKX2 (Lytton J. et al., 2002)

### ***NCKX***

Six different mouse or human NCKX gene products have been described in the literature which would make it the most numerous gene family of Ca<sup>2+</sup> extrusion proteins. A more careful analysis of the six putative NCKX proteins reveals that NCKX6 may be part of a distinct gene family and this is illustrated by the sequence alignment of the alpha 1 and alpha 2 repeats (Altimimi and Schnetkamp, 2007).

### ***Cloning and Tissue Distribution of the five NCKX Isoforms***

Shortly after the first descriptions of the unique Na<sup>+</sup>/Ca<sup>2+</sup> exchange process in vertebrate retina that requires and transports K<sup>+</sup> (Schnetkamp et al., 1989; Cervetto et al., 1989), the rod NCKX1 cDNA was cloned from bovine retina and transcripts appeared to be highly restricted to the retina and

were not found in any other tissues suggesting that NCKX could be a photoreceptor-specific protein (Reiländer et al.,1992). Dahan (Dahan et al.,1991) sought to investigate whether  $K^+$ -dependent  $Na^+/Ca^{2+}$  exchange was evident in other excitable tissue. In rat brain synaptic plasma membrane vesicle preparations, they deduced that  $K^+$  specifically stimulated both  $Na^+$ -gradient dependent  $Ca^{2+}$  efflux from, and  $Ca^{2+}$  influx into brain synaptic plasma membrane vesicles. Moreover, they showed that  $^{86}Rb^+$  was cotransported with  $Ca^{2+}$ , and assuming a stoichiometry of 1  $Ca^{2+}$  and 1  $K^+$  exchange process (as shown in retina), 10–20% of the transporters in their preparation mediated  $Na^+/Ca^{2+}-K^+$  exchange. Interestingly, another report by Kimura et al. (Kimura et al., 1993) also documented  $K^+$ -dependent  $Na^+/Ca^{2+}$  exchange in human platelets. These studies indicated that  $Na^+/Ca^{2+}-K^+$  exchange is likely to be found in other tissues than the retina.

A second NCKX cDNA was cloned by Tsoi (Tsoi et al.,1998) who found widespread distribution of transcripts of NCKX2 in rat brain. Using in situ hybridization, the following regions of adult rat brain were reported to be particularly enriched in transcripts of NCKX2: the deeper layers of the cortex (V and VI), the CA3 pyramidal neurons of the hippocampus, the thalamic medial geniculate nucleus, the pontine nuclei and the reticulotegmental nuclei of pons, and the molecular layer of the cerebellum. The next isoform to be cloned was NCKX3 (Kraev et al., 2001), which proved to also be particularly abundant within the adult brain. It was reported to be particularly prominent in hippocampal CA1 pyramidal cells,

within thalamic nuclei, and molecular layer of the cerebellum; transcripts of NCKX3 displayed a selectively laminar distribution within cortex, with higher expression in large neurons of layer IV. Additionally, transcripts of NCKX3 were reported in abundance in various other excitable body tissues rich in smooth muscle, particularly aorta, intestine, lung, and uterus; notably transcripts of NCKX3 were not detected in heart. NCKX4 was subsequently cloned and its transcripts reported to be uniformly expressed in adult brain, with prominent expression in CA1, CA3, and dentate gyrus of hippocampus, in the granular layer of cerebellum, the anterodorsal nucleus of thalamus, and granule cell layer of olfactory bulb (Li et al., 2002). In addition, transcripts of NCKX4 were abundantly expressed in aorta, lung, and thymus, and at lower levels in a variety of other tissues such as heart, stomach, small intestine, spleen, lymph node, skeletal muscle, kidney and adrenal gland. (Altimimi and Schnetkamp, 2007).

### ***NCKX in the Brain***

With other isoforms of NCKX cloned and transcripts found in abundance in the brain, and in various other animal tissues, it has become evident that these proteins potentially participate in many physiological processes. There are two approaches to investigating the contribution of  $\text{Na}^+/\text{Ca}^{2+}$  exchange in a given cell type. One way is to run the exchanger in its reverse ( $\text{Ca}^{2+}$  import) mode, which is typically accomplished by equimolar substitution of extracellular  $\text{Na}^+$ . In the case of NCKX, the

reverse mode has an absolute dependence on extracellular  $K^+$  (at least when the extracellular substitute for  $Na^+$  ions is  $Li^+$ ), and with a low apparent affinity for extracellular  $K^+$  on the order of 1–5 mM, the contribution of NCKX can be evaluated without major effects on membrane potential induced by high  $K^+$  depolarization (and the possibility of resultant  $Ca^{2+}$  influx through voltage gated  $Ca^{2+}$  channels). The other method of investigating  $Na^+/Ca^{2+}$  exchange physiologically is by measuring cytosolic  $Ca^{2+}$  clearance rates (after imposing cytosolic  $Ca^{2+}$  loads) in the absence of extracellular  $Na^+$ . In both these approaches, data must be evaluated with prudence, since as aforementioned, other cellular  $Ca^{2+}$  handling mechanisms can influence and obscure the contributions of NCKX (or NCX) under investigation.

Following the indication of  $K^+$ -dependent  $Na^+/Ca^{2+}$  exchange in brain by Dahan (Dahan et al., 1991) the next study that illustrated such activity in neurons is that of Boyer (Boyer et al., 1999) In vestibular sensory hair cells of guinea pig, brief (5–10 seconds) substitution of extracellular  $Na^+$  resulted in elevation of cytosolic free  $Ca^{2+}$ , and this elevation was completely dependent on extracellular  $K^+$ . In that study, Boyer et al. also characterized the ion selectivity of the binding site of the exchanger mediating reverse exchange, and found that only  $K^+$ ,  $Rb^+$ , and  $NH_4^+$  supported  $Ca^{2+}$  influx, but not  $Li^+$ , nor  $Cs^+$  (similar to ion selectivity of K-site of NCKX1 and NCKX2 (Schnetkamp and Szerencsei, 1991; Prinsen et al., 2002)). Interestingly, a subsequent study investigating the contribution of  $Na^+/Ca^{2+}$  exchange in the semicircular canal hair cells of frog found no evidence for  $Na^+/Ca^{2+}$  exchange altogether

(Martini et al., 2002). Aside from the difference in species used by the two studies, the latter study of Martini et al. used solutions of different ionic compositions from those used by Boyer et al. for their fluorescence and whole-cell current recordings.

The definitive characterization of  $K^+$ -dependent  $Na^+/Ca^{2+}$  exchange in brain neurons came from the studies of Kiedrowski (Kiedrowski et al., 2002), where they demonstrated extracellular  $K^+$ -dependent  $^{45}Ca$  accumulation in  $Na^+$ -loaded cerebellar granule cells cultured from rat for 9–11 days in vitro. In a subsequent study (Czyz and Kiedrowski, 2002), the same group demonstrated that inhibition of NCX or NCKX independently failed to limit NMDA-induced  $Ca^{2+}$  accumulation in depolarized and glucose-deprived cerebellar granule cells in vitro (to mimic brain ischaemic conditions). But, when both NCX and NCKX were inhibited simultaneously by application of 10  $\mu$ M KB-R7943 and removal of extracellular  $K^+$  respectively, NMDA-induced  $Ca^{2+}$  accumulation and resultant excitotoxicity were limited significantly. A later study from the same lab (Kiedrowski et al., 2004) compared the contributions of NCX and NCKX to  $Na^+/Ca^{2+}$  exchange-mediated  $Ca^{2+}$  influx between neurons of rat cerebellum and forebrain in in vitro culture. In forebrain neurons, inhibiting NCX with 10  $\mu$ M KB-R7943 resulted in ~85% decrease in the cytosolic free  $Ca^{2+}$  elevation rate, while removing extracellular  $K^+$  to inhibit NCKX (when NCX was operational) did not influence the rate of cytosolic free  $Ca^{2+}$  elevation. In cerebellar granule cells, however, inhibiting NCKX decreased the rate of cytosolic free  $Ca^{2+}$  elevation by ~65%. This shows that NCX and NCKX

have differential contributions in different brain neurons; although northern blot analysis of forebrain neurons and cerebellar granule cells did not reveal pronounced differences in the expression of different NCKX isoforms. These studies all implicate NCKX (as well as NCX) as important transporters in physiological regulation of neuronal cytosolic  $\text{Ca}^{2+}$ , and potentially as important therapeutic targets under pathophysiological conditions such as stroke and brain ischaemia.

While all the aforementioned studies relied primarily on elevation of cytosolic  $\text{Ca}^{2+}$  (reverse exchange) to demonstrate the activity of NCKX, Lee (Lee et al., 2002) have demonstrated operational  $\text{K}^+$ -dependent  $\text{Na}^+/\text{Ca}^{2+}$  exchange in clearance of cytosolic  $\text{Ca}^{2+}$  loads in isolated nerve terminals of rat neurohypophysis. In this preparation, NCKX was demonstrated to specifically contribute to  $\text{Ca}^{2+}$  clearance in the neurohypophysial nerve terminal compartment, but not in the cell bodies of the same neurons in brain slices of hypothalamus containing the somata of supraoptic magnocellular neurosecretory cells (Kim et al., 2003). Although, these functional studies do not conclusively indicate which isoform of NCKX is in these nerve terminals, mRNA transcript localization, and immunohistochemical evidence suggest it is NCKX2. NCKX was later shown, by the same group, to be an important  $\text{Ca}^{2+}$  clearance mechanism in another neuronal axon terminal, the Calyx of Held, in the medullary trapezoid body medial nucleus (Kim et al., 2005). In these mammalian large presynaptic terminals, NCKX was deduced to contribute ~42% of the cytosolic  $\text{Ca}^{2+}$  clearance

(for cytosolic  $\text{Ca}^{2+}$  loads up to  $2.5 \mu\text{M}$ ), while NCX and PMCA each contributed 26% and 23% respectively; mitochondria became an important contributor to cytosolic  $\text{Ca}^{2+}$  clearance once cytosolic  $[\text{Ca}^{2+}]$  exceeded  $3 \mu\text{M}$ . It is not yet known which isoform(s) of NCKX (or NCX) are present in the presynaptic axon terminals of the Calyx of Held.

A defined neuronal physiological role for an NCKX isoform was obtained recently by Li (Li et al., 2006) who developed an embryonic NCKX2 knockout mouse. Analysis of isolated and cultured forebrain cortical neurons from NCKX2 knockout mice revealed a decrease in the NCKX-mediated reverse exchange  $\text{Ca}^{2+}$  import by  $\sim 50\%$ ; the remainder of the external  $\text{K}^+$ -dependent component presumably attributed to NCKX3 and NCKX4. Since NCKX expression is particularly prominent in the hippocampus both at the mRNA level (Tsoi et al., 1998), as well as functionally (Kiedrowski L, 2004), the NCKX2 knockout mice were examined for alterations in hippocampal synaptic plasticity, and behavioural measures of learning and memory. Long term potentiation was induced in hippocampal Schaffer collateral/CA1 synapses in brain slices by two 0.5 s bouts of tetanic (100 Hz) stimulation, and then excitatory postsynaptic field potentials (fEPSP) were elicited at baseline stimulation (0.1 Hz). At 30 min post tetanus, the slopes of fEPSPs (calculated from the rising phase of the peak response) measured in hippocampal slices from wild-type mice were increased to 131% of baseline, whereas in NCKX2 knockout littermates, it was significantly reduced to 88%. On the other hand, long term depression (LTD) was elicited by 15 min of stimulation at 1 Hz; comparison of fEPSP responses in

wild-type hippocampal slices revealed that the fEPSP slopes were reduced to 75% of baseline 30 min after the induction of LTD, whereas it was 50% in NCKX2 knockout littermates. Interestingly, these changes in hippocampal synaptic plasticity observed in NCKX2 knockout mice were not accompanied by changes in synaptic transmission, as revealed by the relation of fEPSP slope to stimulus amplitude, nor in presynaptic facilitation, as revealed by a paired-pulse protocol. The aforementioned effects of NCKX2 loss on hippocampal synaptic plasticity were not accompanied by differences in postsynaptic CA1 neuronal responses as revealed by comparisons of various measures of neuronal excitability, such as resting membrane potential, input resistance, nor in action potential spike firing frequency (and associated spike parameters). Behavioural studies of NCKX2 knockout mice displayed normal performance on a rotating rod task (a test of motor learning) with respect to their wild-type littermates, however, NCKX2 knockout mice failed to improve their performance on this task with subsequent trials, while their wild-type littermates were able to do so. In another behavioural test of spatial learning, a moving platform version of the Morris water maze task, wild-type mice showed improvement in their ability to locate a hidden platform when it was in the same location as the previous day, compared with when it was in a novel location; NCKX2 knockout littermates, however, did not show such improvement. (Altimimi and Schnetkamp, 2007).

### ***Ion selectivity and apparent dissociation constants***

(Altimimi and Schnetkamp, 2007).

Most functional data published on NCKX proteins concern the NCKX 1 and 2 isoforms measured in retinal rod outer segments or expressed in cell lines, respectively. A recent study reported very similar ion dependencies for the NCKX3 and 4 isoforms as previously observed for NCKX1 and 2, (Visser et al., 2007) whereas no data have been reported for NCKX5. The key feature of both NCX and NCKX proteins is the absolute selectivity for Na<sup>+</sup> ions over all other alkali cations to initiate Ca<sup>2+</sup> transport (Schnetkamp PPM, 1986) and this includes Li<sup>+</sup> which can replace Na<sup>+</sup> in many other Na<sup>+</sup> channels and transporters. Most studies on NCX and NCKX proteins employ three different methods to assess function: <sup>45</sup>Ca and <sup>86</sup>Rb fluxes (Schnetkamp et al., 1991a; Szerencsei et al., 2001), patch-clamp measurements (Sheng et al., 2000; Dong et al., 2001) and measurement of changes in intracellular free Ca<sup>2+</sup> using fluorescent dyes of the fluo, fura or indo variety (Visser et al., 2007; Altimimi and Schnetkamp, 2007; Kim et al., 2005). In addition, a few studies have used atomic absorption measurements (Altimimi and Schnetkamp, 2007a Szerencsei et al., 2001; Schnetkamp et al., 1989) and metalochromic dyes (arsenazo III) (Schnetkamp PPM, 1986; Schnetkamp et al., 1989).

In this work we preferred the patch-clamp measurements and the usage of FURA.

The external Na<sup>+</sup> dependence of forward exchange has been measured in rod outer segments (NCKX1) or In cell lines expressing NCKX1 or NCKX2 cDNAs; the data reveal a

sigmoidal dependence on the external  $[\text{Na}^+]$  with reported Hill coefficients between 2 and 3 and apparent  $\text{Na}^+$  dissociation constants of 30–50 mM (Sheng et al., 2000; Dong et al., 2001; Schnetkamp PPM, 1991) Similarly,  $\text{Ca}^{2+}$  influx via reverse exchange is absolutely dependent on internal  $\text{Na}^+$  with a Hill coefficient of 2.6 and an apparent  $\text{Na}^+$  dissociation constant of 50 mM (Altimimi and Schnetkamp, 2007).

A critical difference between NCX and NCKX proteins is the requirement for  $\text{Ca}^{2+}$  and  $\text{K}^+$  cotransport for NCKX proteins, whereas no such requirement exists for NCX proteins. As most functional assays to test for NCKX presence or function rely on measurements of reverse exchange, either in situ or in cell lines expressing NCKX cDNAs, it is important to keep in mind that a measurable  $\text{K}^+$ -independent component of  $\text{Ca}^{2+}$  transport has been observed for both NCKX1 and NCKX2 under certain conditions (Prinsen et al., 2000; Schnetkamp et al., 1991b). This is demonstrated most easily when  $\text{Ca}^{2+}$  influx via reverse exchange is measured in extracellular solutions in which  $\text{Na}^+$  is replaced by choline chloride, tetramethylammonium chloride or sucrose as the main osmotic component. Replacement of extracellular  $\text{Na}^+$  with  $\text{Li}^+$  suppresses the  $\text{K}^+$ -independent component of reverse exchange, and for this reason reverse exchange via NCKX proteins is most conveniently measured in an extracellular solution in which  $\text{Li}^+$  is the major cation.  $\text{Rb}^+$  and  $\text{NH}_4^+$  can replace  $\text{K}^+$  in activating forward or reverse exchange mediated by NCKX proteins,  $\text{Cs}^+$  is a very poor substitute, while  $\text{Li}^+$  and  $\text{Na}^+$  cannot replace  $\text{K}^+$  (Schnetkamp and Szerencsei, 1991; Prinsen et al., 2002). Determination of the apparent  $\text{K}^+$

dissociation constants, both *in situ* and in heterologous systems have yielded a range of values between 1 and 10 mM, depending on the specific experimental conditions.  $\text{Ca}^{2+}$  influx into cells can be mediated by a large number of different  $\text{Ca}^{2+}$  permeable channels present in the plasma membrane as well as by NCX proteins found in many cell types. A useful distinguishing feature of NCKX1-4 proteins is the relatively high affinity for extracellular  $\text{Ca}^{2+}$  (1–3  $\mu\text{M}$ ) (Visser et al., 2007; Szerencsei et al., 2001; Sheng et al., 2000; Schnetkamp PPM, 1991) in  $\text{Na}^+$ -free media, a considerably higher affinity than values of 0.2–0.8 mM reported for NCX proteins (Blaustein and Lederer, 1999). (Altimimi and Schnetkamp, 2007).

### ***Pharmacology of NCKX.***

Very little is known about the pharmacology of NCKX proteins. Earlier work on NCKX1 in retinal rod outer segments showed that 3',5' dichlorobenzamil (Nicol et al., 1987), tetracaine and L-cis diltiazem (Schnetkamp PPM, 1989) could block forward exchange at relatively high concentrations, while the same compounds were much more effective in inhibiting cGMP-gated channels present in this preparation. This implies that these compounds are unlikely to serve as useful diagnostics to detect NCKX activity. More recently, three studies have suggested that KB-R7943 is a blocker of NCKX proteins found in platelets (Takano et al., 2001), sea urchin sperm (Su and Vacquier, 2002) and starfish sperm (Islam et al., 2006), whereas no inhibitory action on NCKX2 was found (Iwamoto et al., 2004). It is important to resolve these

apparently conflicting results as several recent studies (Czyz and Kiedrowski, 2002; Kiedrowski et al., 2004; Li et al., 2006) that address the presence of NCX and NCKX in various types of neurons in the brain have used KB-R7943 to selectively eliminate NCX activity and reveal the contribution of putative NCKX isoforms to Na<sup>+</sup>-dependent Ca<sup>2+</sup> fluxes observed in these neurons. (Altimimi and Schnetkamp, 2007).

## AIM OF THE STUDY

Despite NCKX2 importance in  $\text{Ca}^{2+}$  homeostasis and neuronal function in CNS, its role in stroke, a pathological condition characterized by an alteration of  $\text{Na}^+$ ,  $\text{K}^+$ , and  $\text{Ca}^{2+}$  intraneuronal concentrations (Lipton, 1999), has not yet been investigated. Moreover, NCKX2 is highly expressed in cerebral cortex, striatum, and hippocampus, regions involved in the ischemic insult consequent to middle cerebral artery occlusion (MCAO) in human, primates, and rodents. In the present report, to assess NCKX2 role in cerebral ischemia, we first analyzed NCKX2 mRNA and protein expression in the ischemic core and in the ipsilesional nonischemic areas in rats at different time intervals after permanent MCAO (pMCAO). Then, NCKX2 role in the development of ischemic damage was assessed both in rats, in which NCKX2 expression was knocked down by a specific antisense oligodeoxynucleotide (ODN), and in mice, in which *nckx2* gene was knocked-out. Furthermore, to establish mechanistic insights on how the lack of the NCKX2 could affect neuronal survival in stroke, we have reproduced an *in vitro* model mimicking cerebral ischemia, by exposing primary neuronal cultures from *nckx2*<sup>-/-</sup> mice to oxygen-glucose deprivation (OGD) followed by reoxygenation. In this experimental model, intracellular calcium concentrations ( $[\text{Ca}^{2+}]_i$ ) were detected. Finally, NCKX currents ( $I_{\text{NCKX}}$ ), in forward and reverse mode of operation, were recorded by means of patch-clamp technique in *nckx2*<sup>-/-</sup> cortical neurons exposed to hypoxia

# MATERIALS AND METHODS

## ***Experimental groups***

Male Sprague Dawley rats (Charles River, Calco, Italy) weighing 250–270 g and male C57BL/6 *nckx2*<sup>+/+</sup> (Charles River) and *nckx2*<sup>-/-</sup> mice of the same age (8–10 weeks) and weight (22–25 g) were housed in the same diurnal lighting conditions (12 h darkness and 12 h light). Experiments were performed on rats and mice according to the international guidelines for animal research. The researchers who performed surgery, evaluation of ischemic volume and focal and general neurological scores, genotyping of the mice, and treatments of the rats and neuronal cultures were blinded toward the experimental schedule. The experimental protocol was approved by the Animal Care Committee of the “Federico II” University of Naples.

## ***Surgical procedures***

*Osmotic minipump implantation.* Sprague Dawley rats, anesthetized with chloral hydrate (400 mg/kg, i.p.), were put on a stereotaxic frame. An Alzet (Cupertino, CA) osmotic minipump (model 1003D; delivery rate, 1 $\mu$ l/h) was inserted into a subcutaneous pouch under the skin of the neck and was connected via a plastic catheter to the brain infusion cannula placed into the right lateral ventricle. Twenty-four hours after

cannula implantation, pMCAO was induced as previously described (Pignataro et al., 2004b). Antisense, scramble, and sense oligodeoxynucleotides (250  $\mu$ M, 140  $\mu$ g/kg), when infused intracerebroventricularly, did not affect body temperature.

*pMCAO model.*

All rats were anesthetized intraperitoneally with chloral hydrate (400 mg/kg body weight). A 2 cm incision was made vertically between the orbit and the ear, so as to create a small window just over the visibly identified middle cerebral artery (MCA). The left MCA was electrocauterized by means of a bipolar electrocauterizer (Diatermo MB122; G.I.M.A., Milan, Italy) as close as possible to its origin, near the circle of Willis (Tamura et al., 1981). The body temperature was continuously monitored with a rectal probe (Homeothermic Blanket System; Harvard Apparatus, Holliston, MA) and maintained at  $37\pm 0.5$  °C until the end of the surgical procedure.

*Transient middle cerebral artery occlusion model.*

C57BL/6 *nckx2+/+* and *nckx2-/-* mice were subjected to transient middle cerebral artery occlusion (tMCAO) as previously described (Longa et al., 1989). Under an operating stereomicroscope (Nikon SMZ800; Nikon Instruments, Florence, Italy) the right carotid bifurcation was carefully exposed and the external carotid artery (ECA) coagulated distal to the bifurcation. A 5-0 nylon filament, with its tip rounded by heating near a flame, was inserted through the ECA stump and gently advanced (11 mm) into the right internal carotid artery until it blocked the origin of the MCA. The surgical wound was closed and the filament left in place.

After 60 min of MCA occlusion, the filament was gently withdrawn to restore blood flow. Animals were allowed to recover from anesthesia at room temperature.

***Monitoring of arterial blood pressure, CBF, and blood gas concentration.***

Arterial blood pressure was measured through a catheter inserted into the common carotid artery, connected to solid-state pressure transducers (Power lab system; ADI instruments, Castle Hill, Australia) and analyzed by CHART Windows software. Mean arterial blood pressure values, ranging from 82 to 86 mmHg, did not differ significantly between *nckx2<sup>+/+</sup>* and *nckx2<sup>-/-</sup>* mice (Table 1). Cerebral blood flow (CBF) was monitored in the cerebral cortex ipsilesional to the occluded MCA with a laser-Doppler flowmeter (Periflux system, 5000) in all mice and rats used in ischemia experiments (Pignataro et al., 2004b). Laser-Doppler perfusion was monitored, in mice, throughout the 1 h occlusion period and the first 30 min of reperfusion, and in rats, during all the surgical procedure until 30 min after the occlusion to verify the CBF reduction after MCA electrocauterization. Only rats and mice that, after MCAO, reached at least 70% of CBF reduction were included in the experimental groups (Pignataro et al., 2007). CBF reduction induced by MCAO did not differ significantly between *nckx2<sup>+/+</sup>* and *nckx2<sup>-/-</sup>* mice (Table 1). In some of the experimental and control animals, a catheter was inserted into the common carotid artery to measure arterial blood gases with a blood gas analyzer (Rapid Lab 860; Chiron Diagnostic, Emeryville, CA). PaO<sub>2</sub>, PaCO<sub>2</sub>, and pH mean

values did not change between *nckx2* knock-out and wild-type mice (Table 1).

**Table 1. Physiological data (CBF, blood gases, blood pressure) for *nckx2* +/+ and *nckx2* -/- mice**

Genotype	<i>nckx2</i> +/+	<i>nckx2</i> -/-
pH	7.30 ± 0.06	7.22 ± 0.06
pO <sub>2</sub>	97.8 ± 3.8	101.2 ± 2.01
pCO <sub>2</sub>	38.9 ± 0.67	39.7 ± 2.6
CBF reduction (%)	80.6 ± 1.3	81.8 ± 2.9
Mean arterial blood pressure	85.7 ± 3.1	84.1 ± 0.8

***Cerebrovascular anatomy evaluation of *nckx2* +/+ and *nckx2* -/- mice.***

Cerebral macrovascular morphology was assessed by examining the major cerebral blood vessels of the circle of Willis after transcardial perfusion of *nckx2* +/+ and *nckx2* -/- mice with a solution containing gelatine and waterproof Pelikan Ink (9:1), according to the methodology described by Paxinos and Franklin and other authors to evaluate cerebrovascular anatomy (Huang et al., 1994; Scremin, 1995; Paxinos and Franklin, 2000; Lo et al., 2007).

After injection, the entire head was fixed in 10% formalin overnight before brain removal, to prevent deformation of the brain. The dorsal aspect of the brain was acquired using a macro objective to visualize the line of anastomosis between the anterior cerebral artery (ACA) and MCA. To this aim, we calculated the ratio between the area medial to the line of anastomoses and the total dorsal area of the hemisphere

(Maeda et al., 1998). Moreover, the posterior communicating arteries (PComAs) and the basilar artery (BA) were visualized with a 10X objective and imaged on a computer using a high-resolution digital camera to analyze changes in the diameter of the PComAs and BA (Kitagawa et al., 1998). The data were expressed as the ratio between the calculated diameter of PComAs and BA. Image analysis was made using the NIH Image 1.59 software (National Institutes of Health, Bethesda, MD). All values are given as mean  $\pm$  SEM. After this procedure, to analyze the cerebral microvascular density, the brains were cryopreserved and later serially sectioned on a cryostat at  $-20^{\circ}\text{C}$ . Microvascular density was assessed in the frontoparietal cortex and in the striatum in five sets of three sections (25  $\mu\text{m}$  thick) cut 150  $\mu\text{m}$  apart corresponding approximately to plates 12–16 in a mouse brain atlas (Paxinos and Franklin, 2000). Composite images spanning the full depth of the frontoparietal cortex and the entire area of the striatum were obtained using an Axioskop 20 microscope (Zeiss, Oberkochen, Germany) with motorized XYZ stage (Prior, Rockland, MA) equipped with a high-resolution CCD camera. Images were acquired and analyzed using the MCID Elite software to determine the number of Ink-positive capillary profiles that were  $<10\ \mu\text{m}$  in diameter. Cortical and striatal capillary densities were expressed as the mean  $\pm$  SEM of 15 composite images obtained from each brain. Data are expressed as number of capillaries per  $\text{mm}^2$  in 25- $\mu\text{m}$ -thick slices.

### ***RNA expression analysis by real-time PCR***

The ischemic core and the area surrounding the ischemic core, dissected from the ipsilesional hemisphere of sham-operated and ischemic rats at 6, 9, and 72 h after surgery, were frozen on dry ice. Brain samples were ground into powdered dry ice, then GITC solution (4 M guanidinium isothiocyanate, 25 mM Na citrate, 0.5% Sarkosyl, and 0.7%  $\beta$ -mercaptoethanol) was added. Total RNA was extracted and purified as previously described (Matrone et al., 2004). For reverse transcription, 2.0  $\mu$ g of each extracted RNA was digested with DNase and reverse transcribed using iScript cDNA synthesis kit (Bio-Rad, Mississauga, Ontario, Canada). All data were normalized to glyceraldehyde-3-phosphate dehydrogenase (GAPDH) mRNA levels and expressed as percentage of the mRNA levels detected in sham-operated animals. Sequences of the primers used were the following: NCKX2 193 nt forward (F) (382–401), CTGGAGGAGCGAAGGAAAGG; reverse (R) (555–576), TGTGAAAGTTCTGGGGCTGAC; GAPDH 232 nt F (492–513), CAACTTTGGCATCGTGGAAGGG; R (700–723), CAACGGATACATTGGGGGTAGG.

### ***Western blot analysis***

Total protein extracts from dissected areas of ischemic and nonischemic rat brains were obtained and analyzed as previously described (Matrone et al., 2004) at 3, 6, 24, and 72 h after pMCAO. One group of rats received the calpain inhibitor calpeptin (1 mg/kg; EMD Biosciences, San Diego, CA) 1 h before pMCAO induction and was killed 3 h after

ischemia onset to analyze NCKX2 protein expression in the ischemic core and in the remaining ipsilateral nonischemic area. Nitrocellulose membranes were incubated with anti-NCKX2 antibody (1:100 dilution; polyclonal rabbit antibody; Vinci Biochem, Vinci, Italy). In mice, a polyclonal anti-NCKX2 antibody (1:500 dilution) produced by our research group (Department of Biochemistry and Molecular Biology, University of Calgary) was used. The nitrocellulose membranes were washed with 0.1% Tween 20 and incubated with secondary antibodies for 1 h (GE Healthcare, Little Chalfont, UK). Immunoreactive bands were detected with the ECL (GE Healthcare). The optical density of the bands, normalized with that of  $\alpha$ -actin (Sigma, St. Louis, MO), was determined by Chemi-Doc Imaging System (Bio-Rad).

### ***In situ hybridization***

*Tissue preparation for in situ hybridization.*

Rats were killed 24 h after the onset of the pMCAO. The brains, rapidly removed and quickly frozen on powdered dry ice, were stored at -70°C before sectioning. Serial coronal sections of 12  $\mu$ m were cut on a cryostat (Cryo-StarHM560 MV; Microm International, Walldorf, Germany) at the following levels: medial prefrontal cortex (PFC), anterior caudate-putamen (CPu), posterior CPu, and dorsal hippocampus. All sections corresponded approximately to the bregma levels of +3.20 and -0.30 mm, respectively (Paxinos and Watson, 1998). Each slide contained three adjacent sections of each animal. To select identical anatomical levels in control, sham-operated, and ischemic sections, thionin-stained reference

slides were used. Sections were thaw mounted onto gelatin-coated slides and stored at -70°C for subsequent analysis.

*Oligonucleotide probes and radiolabeling.*

The antisense oligonucleotide probes for labeling NCKX2 transcripts (MWG Biotech, Florence, Italy) are listed in Table 2. To maximize probe specificity, the probe sequences were chosen in regions of low nucleotide homology among the different NCKX isoforms. In addition, to maximize the probe stability, those sequences containing guanine and cytosine levels close to 60% and a very low number of oligo duplexes or hairpin stem formations were selected. Hence the sequences were tested for specificity through a BLAST search (<http://www.ncbi.nlm.nih.gov/blast/Blast.cgi>). NCKX2 probe was a 48 b oligodeoxyribonucleotide (Table 2) complementary to bases 2978–3026 of the rat brain NCKX2 mRNA (GenBank accession number AF021923). In our *in situ* hybridization experiments, the NCKX2probe also recognized the unique splice variant described for this gene in rat brain (Tsoi et al., 1998). Radiolabeling of oligonucleotides probes was performed as previously described (Boscia et al., 2006).

**Table 2. *In situ* hybridization NCKX2 antisense probe information**

Probe	GenBank accession number	Position	5'-oligonucleotide sequence-3'	Length	% Identity/gaps <sup>a</sup>
NCKX2	AF021923	2978–3026	AAACAAGACAGCCTAACCCCTCAA CAGATGCCGCACCCCTCCCCGCCCC	48 bp	NCKX3:58/0 NCKX4:52/0

### *Autoradiography.*

Sections from sham-operated and ischemic rats were processed for radioactive *in situ* hybridization as previously described (Boscia et al., 2006). To detect NCKX2 mRNA, the sections were first dried and then exposed to Kodak-Biomax MR Autoradiographic film (GE Healthcare) for 1 week. The autoradiographic signal yielded by the probes was compared with the results obtained with nonradioactive *in situ* hybridization (Tsoi et al., 1998). The specificity of each probe for the three NCKX isoforms, NCKX2, NCKX3, and NCKX4, was further tested by a control experiment using the corresponding sense oligo (negative control).

### *Image analysis.*

Image analysis was performed as previously described (Boscia et al., 2006). Within the PFC region, at the bregma level of +3.20 mm, three regions of interest (ROIs) were defined: PFC1 was placed in the center of the infarct area (core region); PFC2 was equivalent to the periinfarct area; and PFC3 included the cingulate cortex (Fig. 4A). At the bregma level of -0.30 mm, three ROIs were chosen in the cortex (CTX1, CTX2, and CTX3) and one in the striatum (CPu) (Fig. 4G). CTX3 was located outside the infarct area; CTX2 was located in the periinfarct zone; and CTX1 was located within the core lesion area.

### *Data processing.*

Measurements of transmittance within ROIs were converted into relative disintegration per minute (relative dpm) using a calibration curve based on  $^{14}\text{C}$  standard scale coexposed with the sections, and cross-calibrated with  $^{35}\text{S}$ -brain paste

standards containing known amounts of radioactivity. For this purpose a “best-fit” third-degree polynomial was used, as already described (Boscia et al., 2006). Quantitative comparisons among different experimental groups were performed using images from hybridized sections exposed on the same x-ray film sheet. For each individual section, the value of each ROI contralateral to the ischemic side was subtracted from that of the corresponding ipsilesional side. Differences were calculated in the control, sham-operated, and pMCAO-bearing animals. Measurements from 2–3 consecutive sections of each animal were averaged. The data calculated in the control, sham-operated, and ischemic animals were averaged and processed for statistical analysis. Data were analyzed by means of unpaired two-tailed Student’s *t* test. Because no statistically significant difference was found between control and sham-operated animals, the data are presented as a comparison of pMCAO-bearing animals and sham-operated rats.

### ***NeuN immunohistochemistry***

Sham-operated and ischemic slices kept on chromalum-gelatin slide were fixed at room temperature in 4% (w/v) paraformaldehyde in PBS for 30 min. Briefly, slices were washed four times in PBS, treated with 1% (v/v) hydrogen peroxide (H<sub>2</sub>O<sub>2</sub>) in PBS for 5 min, washed three times in PBS, and, finally, preincubated in PBS containing 3% (w/v) bovine serum albumin (Sigma, Milan, Italy) and 0.1% (v/v) Triton-X (Bio-Rad). Then, the sections were incubated with the primary antibody anti-NeuN (1:2000; Millipore, Vimodrone, Italy) at 4°C

overnight, washed six times in PBS, and finally incubated with the biotinylated secondary antibody (1:200; horse anti-mouse IgG; Vector Laboratories, Burlingame, CA) for 2 h at room temperature. Next, they were washed in PBS and processed with the Elite Vectastain avidin–biotin kit (1:300; 1,5 h; Vector Laboratories). The peroxidase reaction was developed by 3–3'-diaminobenzidinetetrahydrochloride (Sigma) as a chromogen. After the final wash, sections were dehydrated and coverslipped. Slices were acquired with a CCD digital camera (C-5985; Hamamatsu Photonics, Milan, Italy) and Image Pro-Plus software (Media Cybernetics, Silver Spring, MD).

### ***Antisense oligodeoxynucleotide design***

A chimeric phosphorothioated antisense ODN (AS-ODN) (Primm, Milan, Italy) was designed to target the area near the start region. NCKX2 antisense was a 20 b oligodeoxynucleotide, complementary to bases 102–121 of the rat brain NCKX2 mRNA (GenBank accession number AF021923). AS-ODN sequence is the following (underlined bases are phosphorothioated): AS-NCKX2 (+102/+121): 5'-CCAATGACTCGAATTAGCTT-3'. Phosphorothioated ODNs display an increased stability and are more easily diffused into the brain when they are intracerebroventricularly infused (Yaida and Nowak, 1995). The AS-ODN was designed on a region of NCKX2 sequence with low homology to the sequence of the other NCKX and NCX isoforms, as resulted from the alignment of NCKX2 with NCKX and NCX sequences. Hence, AS- and scramble ODN sequences were

tested for specificity through a BLAST search (<http://www.ncbi.nlm.nih.gov/blast/Blast.cgi>). Antisense (CCAATGACTCGAATTAGCTT), sense (5'-AAGCTAATTTCGAGTCATTGG-3'), and scramble (TGCACACTTACAACGTAGTT) NCKX2 ODNs were continuously infused in rats (250  $\mu$ M, 140  $\mu$ g/kg, i.c.v.) with osmotic minipumps for 48 h, starting 24 h before pMCAO induction (Pignataro et al., 2004b).

#### *Evaluation of AS-ODN efficacy in vitro and in vivo*

AS-ODN efficacy was evaluated on NGF-differentiated rat pheochromocytoma cells (PC12 cells) at the concentration of 3  $\mu$ M. PC12 cells were grown as previously described (Pannaccione et al., 2005). The AS-ODN entrance into the cells was enhanced by Lipofectamine 2000 (Invitrogen, Milan, Italy). Western blot analysis was performed 12 and 24 h after cell transfection with the antisense. AS-ODN efficacy was tested also *in vivo* by measuring NCKX2 expression by Western blot in male rats treated with AS-ODN (140  $\mu$ g/kg, i.c.v.) infused through an osmotic minipump for 24 h.

#### ***Evaluation of the ischemic volume in rats treated with AS-ODN.***

To evaluate whether AS-ODN could affect the ischemic volume in rats, the antisense was injected continuously for 48 h, starting 24 h before pMCAO induction. Then, the animals were decapitated 24 h after ischemia onset, a time when the extension of infarct was maximal (Tortiglione et al., 2002). The infarct area and the total volume of the lesion were evaluated with 2,3,5-triphenyl tetrazolium chloride staining and

calculated as previously described (Tortiglione et al., 2002). The total infarct volume was expressed as a percentage of the volume of the ipsilesional hemisphere (Pignataro et al., 2004a).

***Evaluation of the ischemic volume and neurological deficits in *nckx2*<sup>+/+</sup> C57BL/6 wild-type mice and *nckx2*<sup>-/-</sup> mice***

*nckx2*<sup>+/+</sup> C57BL/6 and *nckx2*<sup>-/-</sup> male mice (Li et al., 2006), subjected to 1 h of tMCAO, were decapitated 24 h after ischemia onset. The infarct area and the total volume of the lesion were evaluated as previously described (Pignataro et al., 2004a). Twenty-four hours postischemia, each neurological function was scored according to two scales: a general neurological scale (general score, 0–28) and a focal neurological scale (focal score, 0–28) (Clark et al., 1997).

***Primary cortical neurons***

Cortical neurons were prepared from brains of 14-d-old mouse embryos (Charles River), plated on coverslips, and cultured in MEM/F12 (Invitrogen) containing glucose, 5% of deactivated fetal bovine serum and 5% horse serum (Invitrogen), glutamine (2 mM), penicillin (50 U/ml), and streptomycin (50 µg/ml). Cytosine-β-D-arabinofuranoside (10 µM) was added within 5 d of plating to prevent the growth of non-neuronal cells. Neurons were cultured at 37°C in a humidified 5% CO<sub>2</sub> atmosphere and used after 7–10 d *in vitro* (DIV) (Scorziello et al., 2007). Hypoxic conditions were induced by exposing cortical neurons to oxygen- and glucose-free medium in a

humidified atmosphere containing 95% nitrogen and 5% CO<sub>2</sub> (Scorziello et al., 2007). In primary cortical neurons, cell injury was assessed after 3 h of OGD followed by 21 h of reoxygenation. Propidium iodide- (PI; 7  $\mu$ M) and fluorescein diacetate- (FDA; 36  $\mu$ M) positive cells were counted in three representative high-power fields of independent cultures, and cell death was determined by the ratio of the number of PI-positive cells/PI+FDA-stained-positive cells.

### ***[Ca<sup>2+</sup>]<sub>i</sub> measurement***

[Ca<sup>2+</sup>]<sub>i</sub> was measured by single-cell computer-assisted videoimaging (Secondo et al., 2007). Briefly, cortical neurons, grown on glass coverslips, in control conditions and after exposure to 3 h of OGD plus 4, 6, and 21 h of reoxygenation, were loaded with 6  $\mu$ M fura-2 AM (EMD Biosciences) for 30 min at 37°C. At the end of the fura-2 AM loading period, the coverslips were placed into a perfusion chamber (Medical Systems, Greenvale, NY) mounted onto a Zeiss Axiovert 200 microscope equipped with a FLUAR 40X oil objective lens. The experiments were performed with a digital imaging system composed of MicroMax 512BFT cooled CCD camera (Princeton Instruments, Trenton, NJ), LAMBDA 10-2 filter wheeler (Sutter Instruments, Novato, CA), and MetaMorph/MetaFluor Imaging System software (Universal Imaging, West Chester, PA). After loading, cells were alternatively illuminated at wavelengths of 340 and 380 nm by a xenon lamp. The emitted light was passed through a 512 nm barrier filter. Fura-2AM fluorescence intensity was measured every 3 s. Ratiometric values were automatically converted by

the software into  $[Ca^{2+}]_i$  using a preloaded calibration curve obtained in preliminary experiments as previously reported (Grynkiewicz et al., 1985).

### ***Electrophysiology***

$I_{NCKX}$  was recorded from primary *nckx2*<sup>+/+</sup> and *nckx2*<sup>-/-</sup> cortical neurons by the patch-clamp technique in whole-cell configuration. Currents were filtered at 5 kHz and digitized using a Digidata 1322A interface (Molecular Devices, Sunnyvale, CA). Data were acquired and analyzed using the pClamp software (version 9.0; Molecular Devices). Reverse and forward  $I_{NCKX}$  were recorded using a holding potential of 0 mV. The  $I_{NCKX}$  was recorded, according to Dong et al. (2001), starting from a holding potential of 0 mV to a short-step depolarization at +80 mV (60 ms). Then, a descending voltage ramp from +80 mV to -80 mV was applied. The current recorded in the descending portion of the ramp (from +80 mV to -80 mV) was used to plot the current–voltage ( $I$ – $V$ ) relation curve. The magnitude of  $I_{NCKX}$  was measured at the end of +80 mV (reverse mode) and at the end of -80 mV (forward mode), respectively. Current recordings in control conditions, in which  $I_{NCKX}$  were not detectable, were obtained by perfusing cortical neurons with Na<sup>+</sup>-, Ca<sup>2+</sup>-, and K<sup>+</sup>-free bath solution containing the following (in mM): 130 LiCl, 1 MgCl<sub>2</sub>, 10 D-glucose, 10 HEPES, 0.5 EGTA, 20 tetraethylammonium (TEA), 10 μM nimodipine, and 50 nM tetrodotoxin (TTX), pH 7.4. TTX, nimodipine, and TEA were used to block TEA-sensitive K<sup>+</sup>, TTX-sensitive Na<sup>+</sup>, and L-type Ca<sup>2+</sup> currents. To record both reverse and forward  $I_{NCKX}$ , the external solution was varied by

replacing 130mM LiCl with 80mM NaCl and 50mM KCl, and adding 1mM CaCl<sub>2</sub>. The dialyzing pipette solution contained the following (mM): 18 NaCl, 100 potassium gluconate, 20 TEA, 1 MgATP, 10 EGTA, 6.4 CaCl<sub>2</sub>, 10 D-glucose, and 10 HEPES, pH 7.2. Free [Ca<sup>2+</sup>] under these experimental conditions was ≈0.3 μM.  $I_{NCKX}$  was isolated by digital subtraction of currents elicited under conditions where NCKXs were inactive (bath perfusion with Li<sup>+</sup> and lacking Na<sup>+</sup>, Ca<sup>2+</sup>, and K<sup>+</sup> ions) from currents elicited under conditions compatible with NCKXs function (bath perfusion with a solution containing Na<sup>+</sup>, K<sup>+</sup>, and Ca<sup>2+</sup> ions). In these experimental conditions, the reversal potential for  $I_{NCKX}$  was estimated to be -10 mV, which was much greater than the reversal potential reported for  $I_{NCX}$  (-40 mV) (Hilgemann et al., 1991). This large difference between the reversal potential of  $I_{NCKX}$  estimated in the present study and that reported for  $I_{NCX}$ , together with the inhibitory effect on NCX currents exerted by the high external K<sup>+</sup> concentrations (Zhang and Hancox, 2003) used in the present study, allows us to exclude a significant  $I_{NCX}$  contamination of the recorded current. This aspect was further supported by the decrease in the current magnitude observed in *nckx2*<sup>-/-</sup> primary cortical neurons compared with *nckx2*<sup>+/+</sup> cells. Possible changes in cell size occurring after specific treatments were calculated by monitoring the capacitance of each cell membrane, which is directly related to membrane surface area, and by expressing the current amplitude data as current densities (pA/pF). Capacitive currents were estimated from the decay of capacitive transient induced by 5mV depolarizing pulses from a holding potential of -80 mV and

acquired at a sampling rate of 50 kHz. The capacitance of the membrane was calculated according to the following equation:  $C_m = \tau_c \times I_0 / \Delta E_m (1 - I_\infty / I_0)$ , where  $C_m$  is membrane capacitance,  $\tau_c$  is the time constant of the membrane capacitance,  $I_0$  is the maximum capacitance current value,  $\Delta E_m$  is the amplitude of the voltage step, and  $I_\infty$  is the amplitude of the steady-state current.

### ***Statistical analysis***

Values are expressed as mean $\pm$ SEM. Statistical analysis was performed with ANOVA followed by Newman–Keuls test. Neurological deficits data were analyzed using the nonparametric Kruskal–Wallis test. Statistical significance was accepted at the 95% confidence level ( $p < 0.05$ ). Values are expressed as means  $\pm$  SEM.

# RESULTS

## **TIME COURSE OF NCKX2 mRNA EXPRESSION BY REAL-TIME PCR IN THE ISCHEMIC CORE AND IN THE AREA SURROUNDING THE ISCHEMIC CORE AFTER PMCAO IN RATS**

In the ischemic core, NCKX2-mRNA levels displayed a significant decrease (30%) 72 h after pMCAO, compared with the sham operated animals (Fig. 3A). In the ipsilesional area surrounding the ischemic core, a remarkable reduction in NCKX2 (30%) also occurred starting 9 h after pMCAO induction (Fig. 3B), compared with the sham-operated rats. This reduction was still present 72 h later.

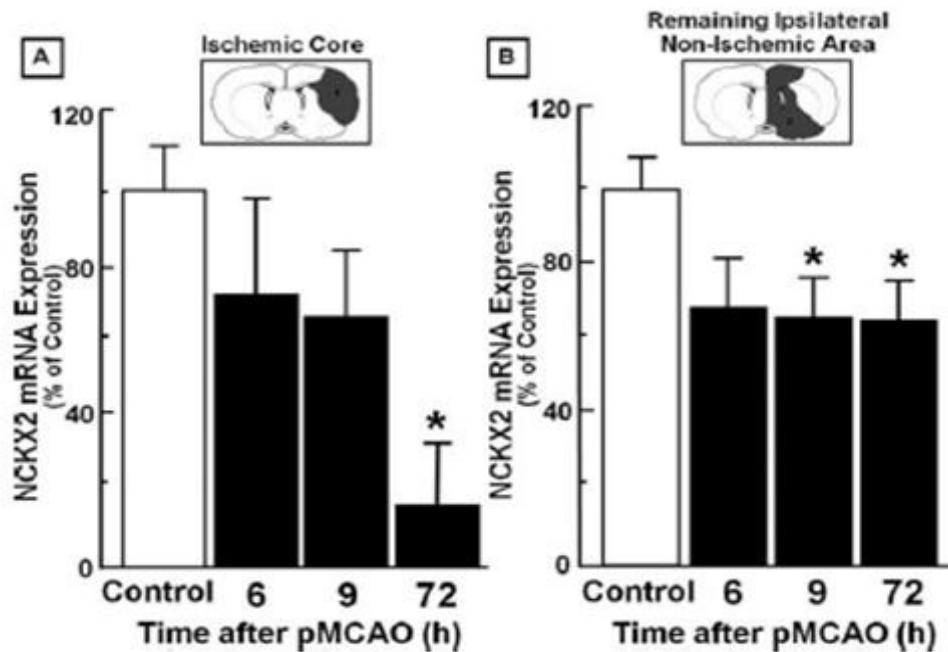


**Fig. 3** Time course of NCKX2 mRNA expression after pMCAO in the ischemic core and in the remaining ipsilateral nonischemic area. **A, B**, Real-time PCR of NCKX2 mRNA expression in the ischemic core (A) and in the remaining ipsilateral nonischemic area (B) are represented. Data were normalized on the basis of GAPDH levels and expressed as a percentage of sham-operated controls, taken as 100%. Values represent means  $\pm$  SEM (n=7).

### **NCKX2 MRNA EXPRESSION IN THE PREFRONTAL CORTEX, CINGULATE, MOTOR AND SOMATOSENSORY CORTICES, AND CAUDATE–PUTAMEN OF SHAM-OPERATED AND PMCAO-BEARING RATS EVALUATED 24 H AFTER PMCAO**

NeuN immunohistochemistry revealed that 24 h after pMCAO, the ischemic damage encompassed the prefrontal (motor and insular compartments), somatosensory (parietal), and insular

cortices, whereas the cingulate and retrosplenial cortices, the caudate–putamen, and the dorsal hippocampus regions were outside the ischemic core and the periinfarct area (Fig. 4C,I). In sham-operated animals, brain distribution of NCKX2 mRNA, obtained by radioactive *in situ* hybridization (Fig. 4D, J), was largely in agreement with previous studies performed with isoforms specific nonradioactive digoxigenin labelled antisense riboprobes (Tsoi et al., 1998). Densitometric measurements of *in situ* hybridization autoradiographs revealed that in the ipsilesional hemisphere, the PFC1 subregion of the prefrontal cortex (an area belonging to the motor function and located in the ischemic core, 3.2 mm ahead of the bregma) displayed a remarkable downregulation ( $-900 \pm 23$  vs  $25 \pm 21$ ) in NCKX2 transcripts at 24 h, compared with sham operated animals (Fig. 4D–F). In the other motor PFC2 subregion, most likely belonging to the periinfarct zone, NCKX2 mRNA decreased significantly ( $-198 \pm 46$  vs  $32 \pm 42$ ) (Fig. 4D–F). No variation in NCKX2 transcripts was detected at 24 h after pMCAO in the PFC3 subregion, a region outside the core and the periinfarct region and corresponding to the motor and cingulate division of the prefrontal cortices (Fig. 4D–F). Twentyfour hours after pMCAO, NCKX2 transcripts were downregulated ( $-858 \pm 35$  versus  $-49 \pm 12$ ) in the infarct area CTX1, corresponding to the insular and somatosensory cortices and located 0.3 mm behind the bregma (Fig. 4J–L). Analogously, in the area most likely corresponding to the periinfarct area, the primary and secondary motor cortices CTX2 displayed a significant decrease ( $-268 \pm 50$  vs  $-12 \pm 27$ ) in NCKX2 transcripts (Fig. 4 J–L). In the cingulate cortex, CTX3, an intact region of the

ipsilesional hemisphere, NCKX2 transcripts displayed no significant changes (Fig. 4J–L). Finally, in the caudate–putamen, a subcortical region that was not affected by pMCAO and in which NCKX2 transcripts are largely distributed, this isoform was remarkably reduced ( $-177 \pm 79$  vs  $12 \pm 35$ ) (Fig. 4J–L). No differences in NCKX2 transcript levels were detected in CTX1, CTX2, CTX3, and CPu regions of the hemisphere contralateral to ischemia compared with the corresponding hemisphere of sham-operated rats.

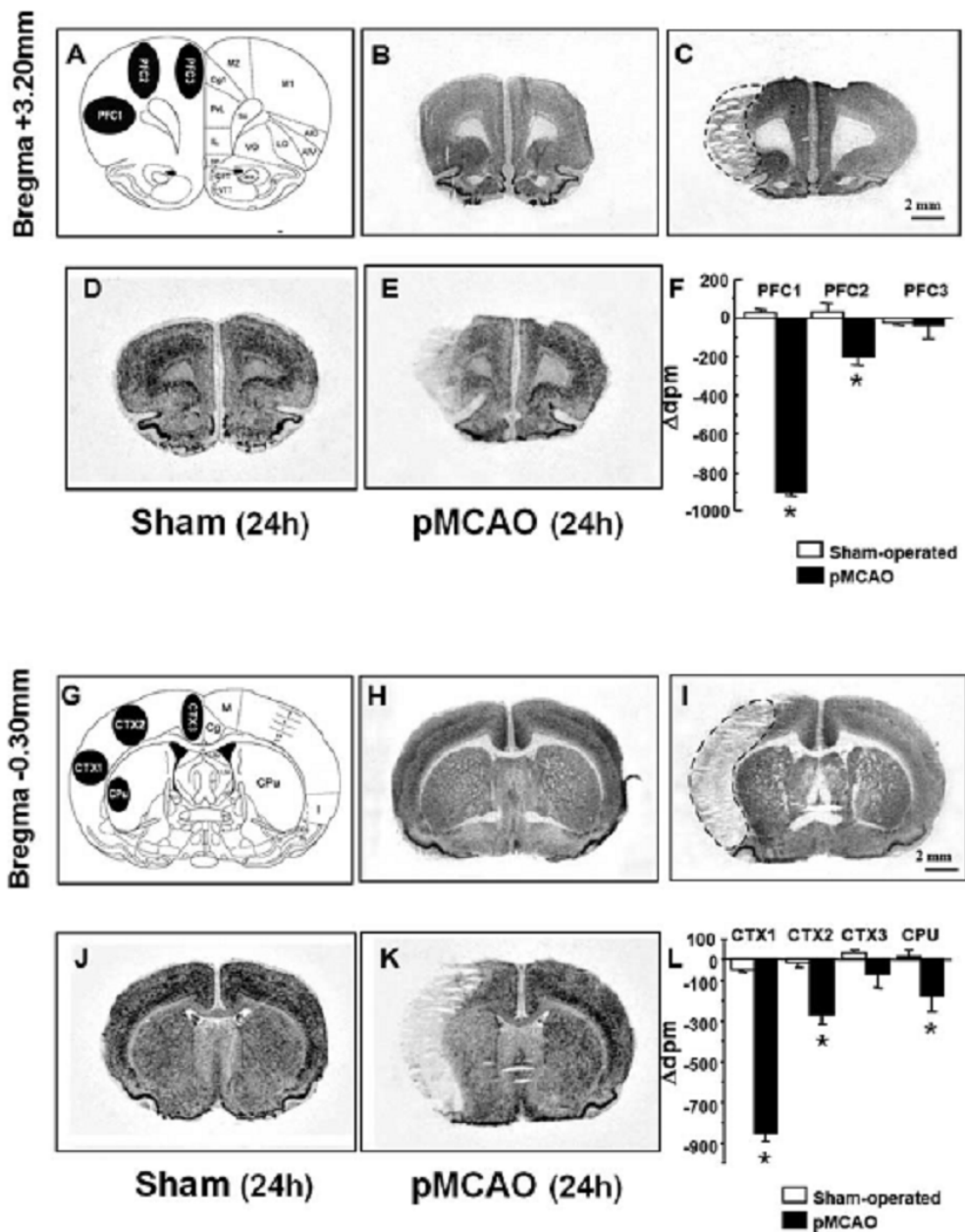


**Fig. 4** Radioactive *in situ* hybridization of NCKX2 transcript in the cerebral cortex and caudate-putamen of Sham-operated and ischemic animals 24h after sham surgery or pMCAO. **A,G**, schematic diagram of regions at coronal bregma levels of +3.20mm and -0.30 mm. Neu-N immunostained sections from sham-operated and pMCAO bearing animals are shown in **B** and **C** (+3.20mm) and **H** and **I** (-0.30mm). **D** and **J** and **E** and **K** represent the *in situ* hybridization autoradiographic film images obtained from sham-operated and ischemic brain sections. mRNA levels expressed as  $\Delta\text{dpm} \pm \text{SEM}$ , with white columns for sham-operated rats and black columns for pMCAO rat, are shown in **F** and **L**.

**TIME COURSE OF NCKX2 PROTEIN EXPRESSION  
EVALUATED BY WESTERN BLOT IN THE ISCHEMIC CORE  
AND IN THE REMAINING IPSILATERAL NONISCHEMIC AREA  
AFTER PMCAO IN RATS**

Analogously to the transcripts levels, in the ischemic core, NCKX2 protein levels were significantly reduced by 50%, compared with control animals, starting 3 h after pMCAO onset. Interestingly, this reduction was still present 72 h later (Fig. 5A). A similar modulation was observed in the ipsilesional area surrounding the ischemic core. Once again, NCKX2 protein levels were reduced by 40%, starting 3 h after pMCAO, and continued to be low 72 h later, compared with control animals (Fig. 5B). In calpeptin-injected rats, NCKX2 downregulation was prevented both in the ischemic core and in the remaining ipsilateral nonischemic area.

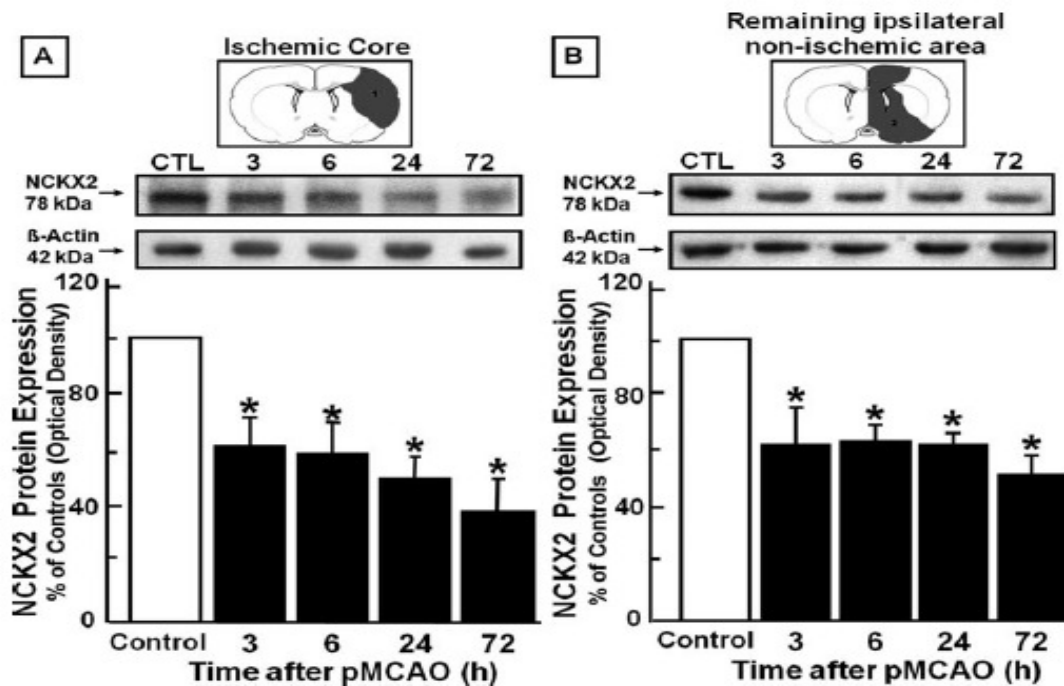


**Fig. 5.** Time course of NCKX2 protein expression after pMCAO in the ischemic core and in the remaining ipsilateral nonischemic area.

## **EFFECT OF NCKX2 KNOCK-DOWN BY ANTISENSE STRATEGY ON THE INFARCT VOLUME INDUCED BY PMCAO IN RATS**

AS-ODN designed against NCKX2 significantly reduced NCKX2 expression in NGF-differentiated PC12 cells. Specifically, the expression was reduced by 20% and by 45% at 12 and 24 h, respectively, after cell treatment with AS-ODN (Fig.6A). A significant reduction (50%) was also observed in vivo in non-ischemic rats in all the brain regions corresponding to the ischemic core and the area surrounding the core 24 h after AS-ODN infusion (Fig. 6B). When the AS-ODN against NCKX2 was infused intracerebroventricularly by means of an osmotic minipump 24 h before pMCAO and for an additional 24 h after the insult, the ischemic volume increased by 32% (Fig. 6C). In contrast, when sense and scramble ODNs were administered for the same time period and at the same concentration, they did not affect the infarct volume. Noticeably, AS-ODN was devoid of direct neurotoxic effects, because its intracerebroventricular infusion did not cause any brain damage in normal rats.

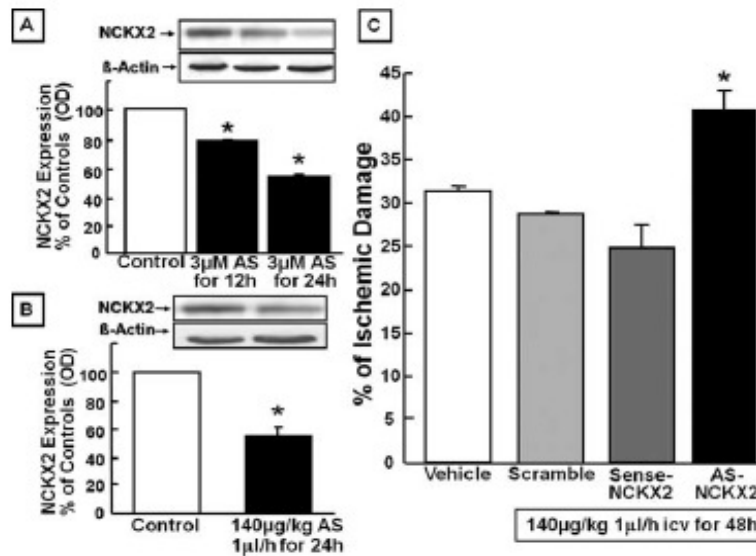


**Fig. 6.** Effect of AS-ODN against NCKX2 on ischemic damage induced in male rats by pMCAO. **A**, Western blot and densitometric analysis of NCKX2 protein in PC12 cells. **B**, Western blot and densitometric analysis of NCKX2 protein after intracerebroventricular infusion of AS-ODN in nonischemic rats. **C**, Effect of Scrambled, Sense or Antisense ODN on infarct volume compared with the ipsilateral hemisphere.

## EFFECT OF NCKX2 KNOCK-OUT ON INFARCT VOLUME AND ON NEUROLOGICAL SCORES INDUCED BY TMCAO IN NCKX2<sup>+/+</sup> AND NCKX2<sup>-/-</sup> MICE

Examination of large cerebral vessels of the ventral brain side did not show anatomical differences in the circle of Willis between *nckx2<sup>+/+</sup>* and *nckx2<sup>-/-</sup>* mice. Similarly, cortical and striatal capillary densities did not show significant variations in the two experimental groups (Fig. 7). Quantitative analysis of the size of the PComA revealed no difference in the ratio between *nckx2<sup>+/+</sup>* (PComA/BA = 0.69 ± 0.16) and *nckx2<sup>-/-</sup>* (PComA/BA = 0.75 ± 0.04) mice. Similarly, the boundary

between ACA and MCA territory, expressed as the percentage ratio between the area medial to the line of anastomoses and the total dorsal area of the hemisphere, was not significantly different between *nckx2*<sup>+/+</sup> (ACA/dorsal area =  $70.9 \pm 2.5\%$ ; *n* = 4) and *nckx2*<sup>-/-</sup> (ACA/dorsal area =  $72.4 \pm 6.8$ ; *n*=4) mice (Fig. 7), thus showing that the MCA and ACA territories are not different between *nckx2* wild-type and knockout mice. Western blot analysis revealed the absence of NCKX2 protein in the brain of *nckx2*<sup>-/-</sup> mice (Fig. 8A). *nckx2* knockout caused a dramatic 130% increase in the extent of the ischemic lesion in *nckx2*<sup>-/-</sup> mice subjected to tMCAO compared with *nckx2*<sup>+/+</sup> mice (Fig. 8B). Interestingly, in parallel with the remarkable increase in ischemic volume induced by *nckk2* knockout, a statistically significant worsening in both general (Fig. 8D) and focal neurological deficits (Fig. 8E) occurred.

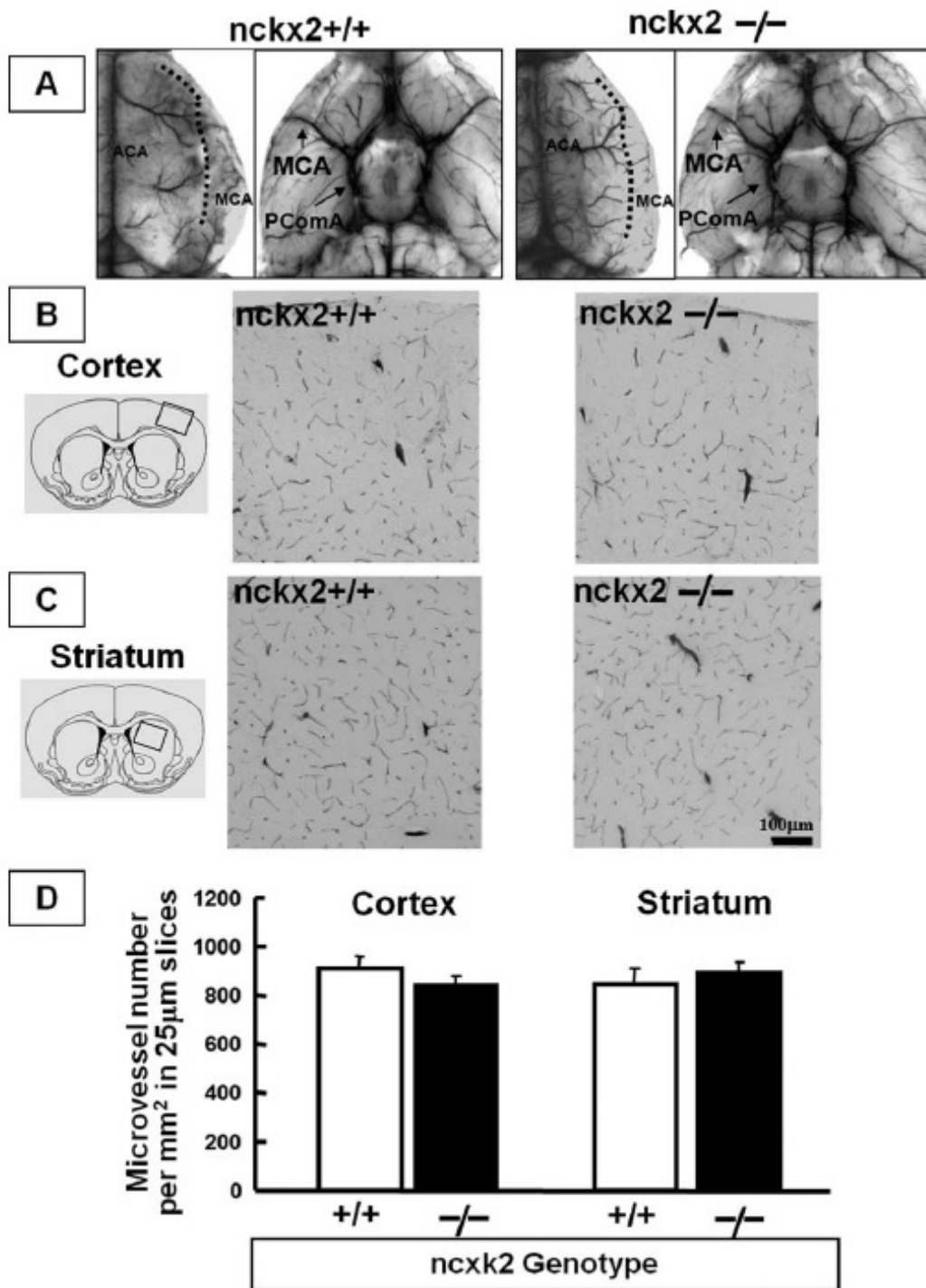


**Fig. 7.** Cerebral vasculature analysis in nckx2<sup>+/+</sup> and nckx2<sup>-/-</sup> mice perfused with Pelikan Ink. **A**, Dorsal and ventral view of large cerebral blood vessels. **B,C**, Microscopic views of microvessel profiles in cortex and striatum of nckx2<sup>+/+</sup> and nckx2<sup>-/-</sup> mice. **D**, Quantification of microvessel numbers per square millimetre in a 25µm-thick slice

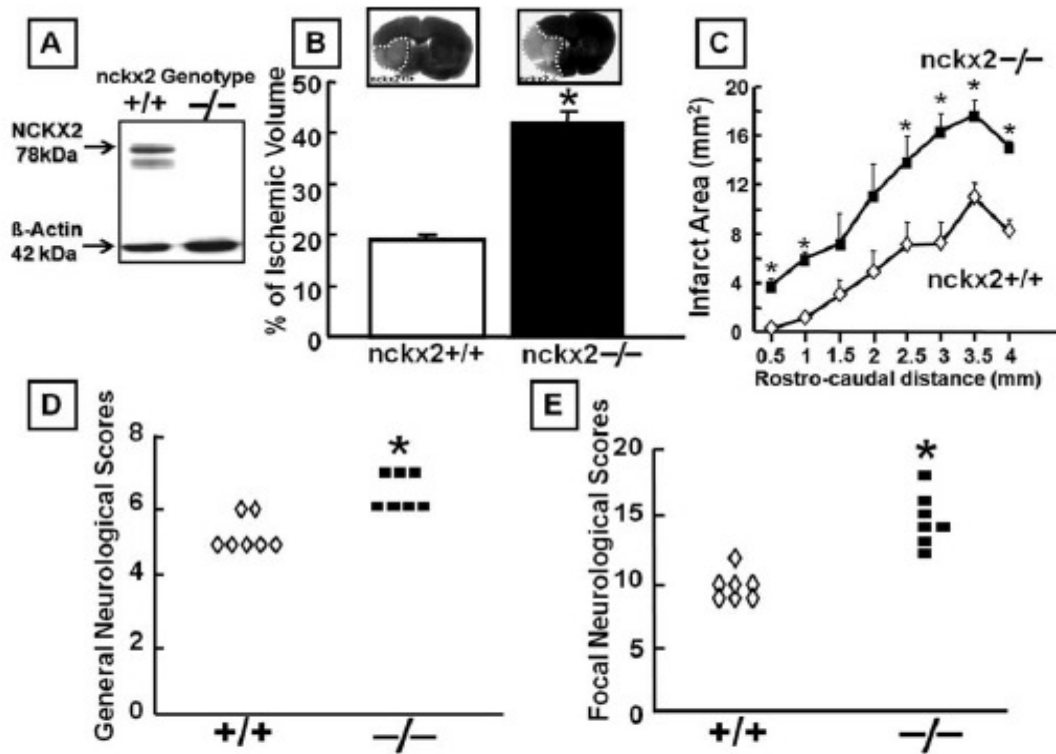


**Fig. 8** **A**, NCKX2 protein expression analyzed by WB in brain tissue from *nckx2*<sup>+/+</sup> and *nckx2*<sup>-/-</sup> mice. **B,C,D,E**, Effect of *nckx2* knock-out on ischemic damage (**B**) and on general (**D**) and focal (**E**) neurological deficits induced by tMCAO in male mice.

## EFFECT OF NCKX2 KNOCK-OUT ON [Ca<sup>2+</sup>]<sub>i</sub> IN CORTICAL NEURONS EXPOSED TO OGD FOLLOWED BY REOXYGENATION

To evaluate the functional role of NCKX2 in the regulation of Ca<sup>2+</sup> homeostasis during hypoxic conditions, [Ca<sup>2+</sup>]<sub>i</sub> was detected by means of fura-2 AM in *nckx2*<sup>+/+</sup> and *nckx2*<sup>-/-</sup> primary cortical neurons exposed to 3 h of OGD followed by reoxygenation. In normoxic conditions, basal levels of [Ca<sup>2+</sup>]<sub>i</sub> were not significantly different between *nckx2*<sup>+/+</sup> and *nckx2*<sup>-/-</sup> cortical neurons [208 nM ± 16.0 (*n* = 65) vs 189 nM ± 4.6 (*n* = 60),

respectively]. In *nckx2*<sup>-/-</sup> primary cortical neurons, 3 h of OGD followed by 4, 6, or 21 h of reoxygenation caused a significantly higher increase in  $[Ca^{2+}]_i$ , at all time intervals, compared with *nckx2*<sup>+/+</sup> cortical neurons (Fig. 9A).

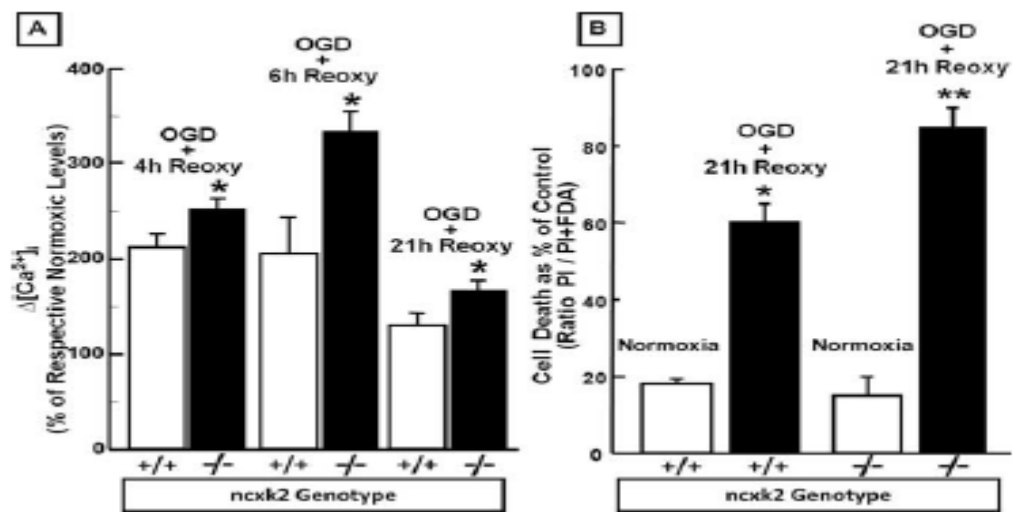


**Fig. 9 A**, Effect of *nckx2* gene ablation on  $[Ca^{2+}]_i$  in cortical neurons from *nckx2*<sup>+/+</sup> and *nckx2*<sup>-/-</sup> mice exposed to OGD followed by 4,6 or 21h of reoxygenation. **B**, Cell death occurring in cortical neurons from *nckx2*<sup>+/+</sup> and *nckx2*<sup>-/-</sup> mice exposed to OGD followed by 21h of reoxygenation.

## EFFECT OF NCKX2 GENETIC ABLATION ON CELL SURVIVAL IN PRIMARY CORTICAL NEURONS EXPOSED TO OGD FOLLOWED BY REOXYGENATION

To further confirm that NCKX2 activity contributes to neuronal protection during brain ischemia, we also investigated whether

primary cortical neurons from *nckx2*<sup>-/-</sup> and *nckx2*<sup>+/+</sup> mice displayed different levels of cell damage when exposed to OGD followed by reoxygenation. In normoxic conditions, cell viability was not different ( $\approx 85\%$ ) between *nckx2*<sup>+/+</sup> and *nckx2*<sup>-/-</sup> primary cortical neurons (Fig. 9B). When 3 h of OGD were followed by 21 h of reoxygenation, *nckx2*<sup>-/-</sup> cortical neurons exhibited a greater rate of cell death than that detected in *nckx2*<sup>+/+</sup> cortical neurons (Fig. 9B).

### **EFFECT OF NCKX2 KNOCK-OUT ON I<sub>NCKX</sub> IN THE FORWARD AND REVERSE MODES OF OPERATION IN PRIMARY CORTICAL NEURONS**

The reversal potential for I<sub>NCKX</sub> in wild-type cortical neurons during normoxic conditions was estimated to be -10 mV. This value was much greater than the reversal potential reported for I<sub>NCX</sub> (-40 mV) (Hilgemann et al., 1991). This large difference between the reversal potential of I<sub>NCKX</sub> estimated in the present study and that reported for I<sub>NCX</sub>, together with the inhibitory effect on NCX currents (Zhang and Hancox, 2003) exerted by the high external K<sup>+</sup> concentrations (50 mM) used in the present study, allows us to exclude a relevant I<sub>NCX</sub> contamination of the recorded I<sub>NCKX</sub>. In normoxic conditions, isolated I<sub>NCKX</sub>, recorded in both the forward and reverse modes of operation in *nckx2*<sup>-/-</sup> primary cortical neurons, was significantly lower than that detected in *nckx2*<sup>+/+</sup> (Fig. 10A,C). It is clear that the current magnitude decreases in the knock-out, so it seems likely that NCKX2 current is part of the current measured. More relevantly, also during anoxic conditions, the

currents carried by NCKX in the forward and reverse modes of operation were significantly reduced in primary cortical neurons obtained from *nckx2*<sup>-/-</sup> mice compared with wild-type mice (Fig. 10B,C). Intriguingly,  $I_{\text{NCKX}}$  recorded in the forward mode of operation after anoxia followed by reoxygenation was significantly lower in *nckx2*<sup>-/-</sup>-cortical neurons than in normoxic *nckx2*<sup>-/-</sup> neurons (Fig. 10C).

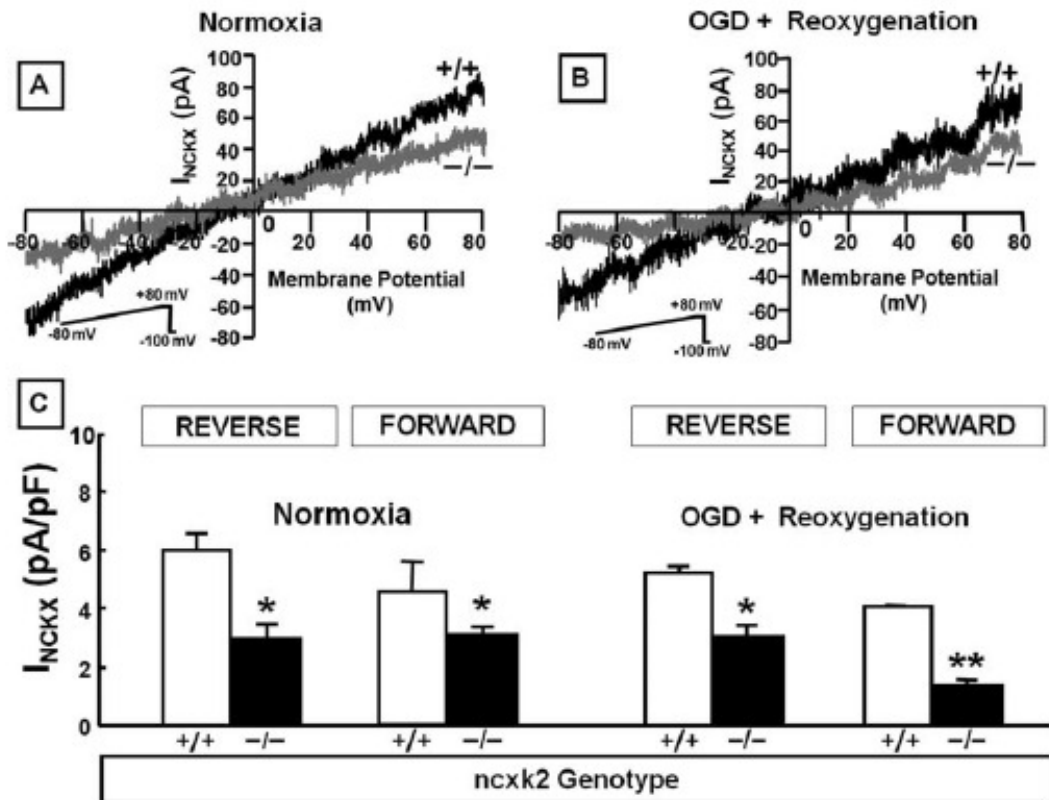


**Fig. 10** Effect of *nckx2* knock-out on  $I_{NCKX}$  recorded in cortical neurons from *nckx2*<sup>+/+</sup> (black tray) or *nckx2*<sup>-/-</sup> (gray trace) under normoxic conditions (**A**) and after 3h OGD followed by 4h reoxygenation (**B**). **C**, Quantification of **A** and **B** expressed as pA/pF

## CONCLUSION AND DISCUSSION

The results of the present study clearly demonstrated for the first time that both knocking down and knocking out NCKX2 expression dramatically increased the extent of the ischemic lesion in rats and mice subjected to pMCAO and tMCAO, respectively. Interestingly, the enlargement of the infarct observed in *nckx2* knock-out mice was associated with a worsening of focal and general neurological deficits. Moreover, focal cerebral ischemia caused relevant changes in the pattern of both NCKX2 mRNA and protein expression in the ischemic core and in the remaining ipsilateral nonischemic area. In accordance with the *in vivo* data, we found that *nckx2*<sup>-/-</sup> primary cortical neurons displayed a higher vulnerability to hypoxic conditions compared with *nckx2*<sup>+/+</sup> cells. In particular,  $[Ca^{2+}]_i$  significantly increased in *nckx2*<sup>-/-</sup> neurons compared with that detected in *nckx2*<sup>+/+</sup> cortical neurons exposed to OGD followed by reoxygenation. In addition, under hypoxic conditions,  $I_{NCKX}$  recorded in the forward and reverse modes of operation in *nckx2*<sup>-/-</sup> neurons was significantly lower than that recorded in *nckx2*<sup>+/+</sup> cortical neurons. All these findings indicate that the disruption of *nckx2* gene by genetic manipulation renders neurons more susceptible to the ischemic insult and that NCKX2 activity attenuates the development of brain injury elicited by ischemia in those cerebral territories supplied by MCA. Furthermore, the critical

role of NCKX2 during ischemia was highlighted by the increase in the infarct volume obtained in two different rodent models of pMCAO and tMCAO. Interestingly, enlargement of the ischemic lesion was also observed when NCKX2 expression was only partially reduced following AS-ODN treatment. The dramatic consequences in the development of ischemic damage and in the death of cortical neurons after *nckx2* ablation might be attributed to the relevant role that NCKX2 can play compared with the other members of the NCX superfamily in extruding calcium ions when it operates in the forward mode. In fact, this K<sup>+</sup>-dependent exchanger isoform, unlike NCKX3 and NCKX4, may be only activated when extracellular K<sup>+</sup> concentrations overcome the physiological levels, being provided with a *K<sub>d</sub>* of ≈40mM (Lee et al., 2002; Visser et al., 2007). Interestingly, during the early phases of brain ischemia, extracellular K<sup>+</sup> concentrations reach, in the ischemic core, levels higher than those corresponding to the *K<sub>d</sub>* of external K<sup>+</sup>-binding sites for NCKX2 (Gido et al., 1997; Visser et al., 2007). That NCKX2 might work in the forward mode during hypoxia is supported by the electrophysiological results obtained in the present study and showing that *I<sub>NCKX</sub>*, recorded in the forward mode of operation, was significantly reduced in anoxic *nckx2*<sup>-/-</sup> cortical neurons, compared with *nckx2*<sup>+/+</sup>. This suggests that during hypoxia, the currents carried by NCKX2 operating in the forward mode play a relevant role in the pathogenesis of the ischemic damage. Accordingly, we found that a remarkable elevation of [Ca<sup>2+</sup>]<sub>i</sub> and a consequent neuronal death occurred in cortical *nckx2*<sup>-/-</sup> neurons. However, we

cannot exclude that, in some brain regions closer to the territory supplied by MCA, and in some stages of the ischemic process, the transmembrane ionic gradients of  $\text{Na}^+$ ,  $\text{K}^+$ , and  $\text{Ca}^{2+}$  might favor NCKX2 to operate in the reverse mode, thus causing the extrusion of  $\text{Na}^+$  ions and the influx of  $\text{K}^+$  and  $\text{Ca}^{2+}$  ions. Indeed, the electrophysiological experiments of the present study demonstrated that, also in the reverse mode of operation, NCKX was lower in *nckx2*<sup>-/-</sup> than in *nckx2*<sup>+/+</sup> cortical neurons exposed to hypoxia. However, it should be underlined that the increase in extracellular  $\text{K}^+$  that is associated with spreading depression, a phenomenon occurring during the ischemic process, may activate this potassium-dependent exchanger, which, in turn, might contribute to attenuate subsequent waves of depolarization. In this way, knocking down and knocking out of NCKX2 might enhance the phenomenon of spreading depression and could account for the increase in infarct volume. As far as the mechanisms responsible for the NCKX2 protein downregulation after brain ischemia are concerned, NCKX2 reduction in the ischemic core and in the remaining ipsilateral nonischemic area could be ascribed to its cleavage by proteolytic enzymes, which are activated during anoxia, as it has been demonstrated for another member of the NCX superfamily, NCX3 (Bano et al., 2005). This hypothesis is supported by our findings showing that NCKX2 downregulation was prevented by the treatment with the calpain inhibitor calpeptin 3 h after pMCAO. Finally, it should be also underlined that we have previously demonstrated that the selective knock-down of the two  $\text{K}^+$ - independent members

of the cation/ $\text{Ca}^{2+}$  exchanger superfamily, NCX1 and NCX3, exacerbates the ischemic damage (Pignataro et al., 2004b, Secondo et al., 2007).

Overall, our results indicate that NCKX2 has a nonredundant role in the maintenance of  $\text{Ca}^{2+}$  homeostasis during conditions of high extracellular  $\text{K}^+$  concentration, because it occurs in neurons during cerebral ischemia. Therefore, NCKX2 emerges as a new potential target to be investigated in the study of the molecular mechanisms involved in cerebral ischemia.

## REFERENCES

Altimimi HF, Schnetkamp PPM (2007a) Na<sup>+</sup>-dependent inactivation of the retinal cone/brain Na<sup>+</sup>/Ca<sup>2+</sup>-K<sup>+</sup> exchanger NCKX2. *J Biol Chem* 282:3720-9.

Altimimi H F, Schnetkamp PPM (2007b) Na<sup>+</sup>/Ca<sup>2+</sup>-K<sup>+</sup> Exchangers (NCKX). Functional Properties and Physiological Roles. *Channels (Austin)*. Mar-Apr;1(2):62-9 Review.

Annunziato L, Pignataro G, Di Renzo GF (2004) Pharmacology of brain Na<sup>+</sup>/Ca<sup>2+</sup> exchanger: from molecular biology to therapeutic perspectives. *Pharmacol Rev* 56:633– 654.

Bano D, Young KW, Guerin CJ, Lefevre R, Rothwell NJ, Naldini L, Rizzuto R, Carafoli E, Nicotera P (2005) Cleavage of the plasma membrane Na<sup>+</sup>/Ca<sup>2+</sup> exchanger in excitotoxicity. *Cell* 120:275–285.

Blaustein MP, Lederer WJ (1999) Sodium/calcium exchange: its physiological implications. *Physiol Rev* 79:763– 854.

Boscia F, Gala R, Pignataro G, de Bartolomeis A, Cicale M, Ambesi-Impiombato A, Di Renzo G, Annunziato L (2006) Permanent focal brain ischemia induces isoform-dependent changes in the pattern of Na<sup>+</sup>/Ca<sup>2+</sup> exchanger gene expression in the ischemic core, periinfarct area, and intact brain regions. *J Cereb Blood Flow Metab* 26:502–517.

Boyer C, Sans A, Vautrin J, Chabbert C, Lehouelleur J (1999) K<sup>+</sup>-dependence of Na<sup>+</sup>-Ca<sup>2+</sup> exchange in type I vestibular sensory cells of guinea-pig. *Eur J Neurosci* 11:1955-9.

Cai X, Lytton J (2004) The cation/Ca<sup>2+</sup> exchanger superfamily: phylogenetic analysis and structural implications. *Mol Biol Evol* 21:1692–1703.

Cervetto L, Lagnado L, Perry RJ, Robinson DW, McNaughton PA (1989) Extrusion of calcium from rod outer segments is driven by both sodium and potassium gradients. *Nature* 337:740-3.

Clark WM, Lessov NS, Dixon MP, Eckenstein F (1997) Monofilament intraluminal middle cerebral artery occlusion in the mouse. *Neurol Res* 19:641–648.

Dahan D, Spanier R, Rahamimoff H (1991) The modulation of rat brain Na<sup>+</sup>-Ca<sup>2+</sup> exchange by K<sup>+</sup>. *J Biol Chem* 266:2067-75.

Dong H, Light PE, French RJ, Lytton J (2001) Electrophysiological characterization and ionic stoichiometry of the rat brain K<sup>+</sup>-dependent Na<sup>+</sup>/Ca<sup>2+</sup> exchanger, NCKX2. *J Biol Chem* 276:25919–25928.

Gido G, Kristian T, Siesjo BK (1997) Extracellular potassium in a neocortical core area after transient focal ischemia. *Stroke* 28:206–210.

Graham D. I., and Brierly, J. B. (1984) Vascular disorders of the central nervous system. In J. H. Adams, J. A. N. Corsellis and L. W. DuChen.(eds), *Greenfield's Neuropathology*. New York: John Wiley & Sons, pp. 157–207.

Grynkiewicz G, Poenie M, Tsien RY (1985) A new generation of Ca<sup>2+</sup> indicators with greatly improved fluorescence properties. *J Biol Chem* 260:3440–3450.

Haddad G.G and Jiang. C (1997) O<sub>2</sub>-sensing mechanisms in excitable cells: Role of plasma membrane K<sup>+</sup> channels *Annu. Rev. Physiol.* 59: 23-43.

Hilgemann DW, Nicoll DA, Philipson KD (1991) Charge movement during  $\text{Na}^+$  translocation by native and cloned cardiac  $\text{Na}^+/\text{Ca}^{2+}$  exchanger. *Nature* 352:715–718.

Huang Z, Huang PL, Panahian N, Dalkara T, Fishman MC, Moskowitz MA (1994) Effects of cerebral ischemia in mice deficient in neuronal nitric oxide synthase. *Science* 265:1883–1885.

Kiedrowski L, Czyz A, Li XF, Lytton J (2002) Preferential expression of plasmalemmal K-dependent  $\text{Na}^+/\text{Ca}^{2+}$  exchangers in neurons versus astrocytes. *Neuroreport* 13:1529-32.

Kiedrowski L (2004) High activity of K<sup>+</sup>-dependent plasmalemmal  $\text{Na}^+/\text{Ca}^{2+}$  exchangers in hippocampal CA1 neurons. *Neuroreport* 15:2113-6.

Kim MH, Lee SH, Park KH, Ho WK (2003) Distribution of K<sup>+</sup>-dependent  $\text{Na}^+/\text{Ca}^{2+}$  exchangers in the rat supraoptic magnocellular neuron is polarized to axon terminals. *J Neurosci* 23:11673–11680.

Kim MH, Korogod N, Schneggenburger R, Ho WK, Lee SH (2005) Interplay between  $\text{Na}^+/\text{Ca}^{2+}$  exchangers and mitochondria in  $\text{Ca}^{2+}$  clearance at the calyx of Held. *J Neurosci* 25:6057– 6065.

Kimura M, Aviv A, Reeves JP (1993) K<sup>+</sup>-dependent  $\text{Na}^+/\text{Ca}^{2+}$  exchange in human platelets. *J Biol Chem* 268:6874-7.

Kitagawa K, Matsumoto M, Yang G, Mabuchi T, Yagita Y, Hori M, Yanagihara T (1998) Cerebral ischemia after bilateral carotid artery occlusion and intraluminal suture occlusion in mice: evaluation of the patency of the posterior communicating artery. *J Cereb Blood Flow Metab* 18:570 –579.

Kraev A, Quednau BD, Leach S, Li XF, Dong H, Winkfein R, Perizzolo M, Cai X, Yang R, Philipson KD, Lytton J (2001) Molecular cloning of a third member of the potassium-dependent sodium-calcium exchanger gene family, NCKX3. *J Biol Chem* 276:23161–23172.

Kristian T and Siesjo B.K. (1997). Changes in ionic fluxes during cerebral ischaemia. *Int. Rev. Neurobiol.* 40: 27-45.

Lamason RL, Mohideen MA, Mest JR, Wong AC, Norton HL, Aros MC, Jurynech MJ, Mao X, Humphreville VR, Humbert JE, Sinha S, Moore JL, Jagadeeswaran P, Zhao W, Ning G, Makalowska I, McKeigue PM, O'Donnell D, Kittles R, Parra EJ, et al. (2005) SLC24A5, a putative cation exchanger, affects pigmentation in zebrafish and humans. *Science* 310:1782–1786.

Lee SH, Kim MH, Park KH, Earm YE, HoWK (2002) K<sup>+</sup>-dependent Na<sup>+</sup>/Ca<sup>2+</sup> exchange is a major Ca<sup>2+</sup> clearance mechanism in axon terminals of rat neurohypophysis. *J Neurosci* 22:6891– 6899.

Li XF, Kraev AS, Lytton J (2002) Molecular cloning of a fourth member of the potassium-dependent sodium–calcium exchanger gene family, NCKX4. *J Biol Chem* 277:48410–48417.

Li XF, Kiedrowski L, Tremblay F, Fernandez FR, Perizzolo M, Winkfein RJ, Turner RW, Bains JS, Rancourt DE, Lytton J (2006) Importance of K<sup>+</sup>- dependent Na<sup>+</sup>/Ca<sup>2+</sup>-exchanger 2, NCKX2, in motor learning and memory. *J Biol Chem* 281:6273– 6282.

Li Z, Matsuoka S, Hryshko LV, Nicoll DA, BersohnMM, Burke EP, Lifton RP, Philipson KD (1994) Cloning of the NCX2 isoform of the plasma membrane Na<sup>+</sup>/Ca<sup>2+</sup> exchanger. *J Biol Chem* 269:17434 –17439.

Lipton P (1999) Ischemic cell death in brain neurons. *Physiol Rev* 79:1431–1568.

Lo AC, Cheung AK, Hung VK, Yeung CM, He QY, Chiu JF, Chung SS, Chung SK (2007) Deletion of aldose reductase leads to protection against cerebral ischemic injury. *J Cereb Blood Flow Metab* 27:1496 – 1509.

Longa EZ, Weinstein PR, Carlson S, Cummins R (1989) Reversible middle cerebral artery occlusion without craniectomy in rats. *Stroke* 20:84 –91.

Lytton J, Li XF, Dong H, Kraev A (2002) K<sup>+</sup>-dependent Na<sup>+</sup>/Ca<sup>2+</sup> exchangers in the brain. *Ann NY Acad Sci* 976:382–393.

Maeda K, Hata R, Hossmann KA (1998) Differences in the cerebrovascular anatomy of C57black/6 and SV129 mice. *NeuroReport* 9:1261–1265.

Martini M, Rossi ML, Farinelli F, Moriondo A, Mammano F, Rispoli G (2002). No evidence for calcium electrogenic exchanger in frog semicircular canal hair cells. *Eur J Neurosci* 16:1647-53.

Matrone C, Pignataro G, Molinaro P, Irace C, Scorziello A, Di Renzo GF, Annunziato L (2004) HIF-1 $\alpha$  reveals a binding activity to the promoter of iNOS gene after permanent middle cerebral artery occlusion. *J Neurochem* 90:368 –378.

Nicoll DA, Longoni S, Philipson KD (1990) Molecular cloning and functional expression of the cardiac sarcolemmal Na<sup>+</sup>/Ca<sup>2+</sup> exchanger. *Science* 250:562–565.

Nicholls D and Attwell D (1990) The release and uptake of excitatory amino acids *Trends Pharmacol. Sci.* 11: 462-468..

Nicoll DA, Hryshko LV, Matsuoka S, Frank JS, Philipson KD (1996) Mutation of amino acid residues in the putative transmembrane segments of the cardiac sarcolemmal  $\text{Na}^+/\text{Ca}^{2+}$  exchanger. *J Biol Chem* 271:13385–13391.

Ogawa S, Kitao Y, Hori O (2007) Ischemia-Induced Neuronal Cell Death and Stress Response. Review. *Antioxidants & Redox Signaling* 9 (5):573-587.

Pannaccione A, Secondo A, Scorziello A, Cali G, Tagliatela M, Annunziato L (2005) Nuclear factor-kappaB activation by reactive oxygen species mediates voltage-gated  $\text{K}^+$  current enhancement by neurotoxic betaamyloid peptides in nerve growth factor-differentiated PC-12 cells and hippocampal neurones. *J Neurochem* 94:572–586.

Paxinos G, Franklin KBJ (2000) *The mouse brain stereotaxic coordinates*. New York: Academic.

Paxinos G, Watson C (1998) *The rat brain in stereotaxic coordinates*. New York: Academic.

Philipson KD, Nishimoto AY (1981) Efflux of  $\text{Ca}^{2+}$  from cardiac sarcolemmal vesicles: Influence of external  $\text{Ca}^{2+}$  and  $\text{Na}^+$ . *J Biol Chem* 256:3698-702.

Pignataro G, Gala R, Cuomo O, Tortiglione A, Giaccio L, Castaldo P, Sirabella R, Matrone C, Canitano A, Amoroso S, Di Renzo G, Annunziato L (2004a) Two sodium/calcium exchanger gene products, NCX1 and NCX3, play a major role in the development of permanent focal cerebral ischemia. *Stroke* 35:2566 –2570.

Pignataro G, Tortiglione A, Scorziello A, Giaccio L, Secondo A, Severino B, Santagada V, Caliendo G, Amoroso S, Di Renzo G, Annunziato L (2004b) Evidence for a protective role played by the  $\text{Na}^+/\text{Ca}^{2+}$  exchanger

in cerebral ischemia induced by middle cerebral artery occlusion in male rats. *Neuropharmacology* 46:439–448.

Pignataro G, Simon RP, Xiong ZG (2007) Prolonged activation of ASIC1a and the time window for neuroprotection in cerebral ischaemia. *Brain* 130:151–158.

Prinsen CFM, Szerencsei RT, Schnetkamp PPM (2000) Molecular cloning and functional expression of the potassium-dependent sodium–calcium exchanger from human and chicken retinal cone photoreceptors. *J Neurosci* 20:1424 –1434.

Prinsen CFM, Cooper CB, Szerencsei RT, Murthy SK, Demetrick DJ, Schnetkamp PPM (2002) The retinal rod and cone Na<sup>+</sup>/Ca<sup>2+</sup>-K<sup>+</sup> exchangers. *Adv Exp Med Biol* 2002; 514:237-51.

Purves D, Augustine G J, Fitzpatrick D K, Lawrence C, LaMantia A S, McNamara J O; Williams S M (2001). *Neuroscience*. Sunderland (MA): Sinauer Associates, Inc.

Reeves JP (1985) The sarcolemmal sodium-calcium exchange system. *Curr Top Membr Transp* 25:77-127.

Reilander H, Achilles A, Friedel U, Maul G, Lottspeich F, Cook NJ (1992) Primary structure and functional expression of the Na/Ca,K-exchanger from bovine rod photoreceptors. *EMBO J* 11:1689 –1695.

Schnetkamp PPM (1980) Ion selectivity of the cation transport system of isolated cattle rod outer segments. *Biochim Biophys Acta* 598:66-90.

Schnetkamp PPM (1986) Sodium-Calcium exchange in the outer segments of bovine rod photoreceptors. *J Physiol* 373:25-45.

Schnetkamp PPM (1989). Na-Ca or Na-Ca-K exchange in the outer segments of vertebrate rod photoreceptors. *Prog Biophys Mol Biol* 54:1-29.

Schnetkamp PPM, Szerencsei RT, Basu DK (1991a) Unidirectional Na<sup>+</sup>, Ca<sup>2+</sup> and K<sup>+</sup> fluxes through the bovine rod outer segment Na-Ca-K exchanger. *J Biol Chem* 266:198-206.

Schnetkamp PPM, Li XB, Basu DK, Szerencsei RT (1991b) Regulation of free cytosolic Ca<sup>2+</sup> concentration in the outer segments of bovine retinal rods by Na-Ca-K exchange measured with Fluo-3. I. Efficiency of transport and interactions between cations. *J Biol Chem* 266:22975-82.

Schnetkamp PPM, Szerencsei RT (1991) Effect of potassium ions and membrane potential on the Na-Ca-K exchanger in isolated intact bovine rod outer segments. *J Biol Chem* 266:189-97.

Schnetkamp PPM (1991) Optical measurements of Na-Ca-K exchange currents in intact outer segments isolated from bovine retinal rods. *J Gen Physiol* 98:555-73.

Schwarz EM, Benzer S (1997) Calx, a Na<sup>+</sup>/Ca<sup>2+</sup> exchanger gene of *Drosophila melanogaster*. *Proc Natl Acad Sci USA* 94:10249–10254.

Scorziello A, Santillo M, Adornetto A, Dell'aversano C, Sirabella R, Damiano S, Canzoniero LM, Renzo GF, Annunziato L (2007) NO-induced neuroprotection in ischemic preconditioning stimulates mitochondrial Mn-SOD activity and expression via RAS/ERK1/2 pathway. *J Neurochem* 103:1472–1480.

Scremin OU (1995) Cerebral vascular system. In: *The rat nervous system* (Paxinos G, ed), pp 3–35. New York: Academic.

Secondo A, Staiano RI, Scorziello A, Sirabella R, Boscia F, Adornetto A, Valsecchi V, Molinaro P, Canzoniero LM, Di Renzo G, Annunziato L (2007) BHK cells transfected with NCX3 are more resistant to hypoxia followed by reoxygenation than those transfected with NCX1 and NCX2: possible relationship with mitochondrial membrane potential. *Cell Calcium* 42:521–535.

Sheng JZ, Prinsen CFM, Clark RB, Giles WR, Schnetkamp PPM (2000) Na<sup>+</sup>-Ca<sup>2+</sup>-K<sup>+</sup> currents measured in insect cells transfected with the retinal cone or rod Na<sup>+</sup>-Ca<sup>2+</sup>-K<sup>+</sup> exchanger cDNA. *Biophys J* 79:1945-53.

Siegel G. J.; Agranoff, B. W.; Albers, R. W.; Fisher, S. K.; Uhler, M D. (1999) *Basic Neurochemistry: Molecular, Cellular, and Medical Aspects*. editors Philadelphia: Lippincott, Williams & Wilkins.

Siesjoe BK (1988) Mechanisms of ischemic brain damage. *Crit Care Med* 16: 954–963.

Szerencsei RT, Prinsen CFM, Schnetkamp PPM (2001) The stoichiometry of the retinal cone Na/Ca-K exchanger heterologously expressed in insect cells: Comparison with the bovine heart Na/Ca exchanger. *Biochemistry* 40:6009-15.

Tamura A, Graham DI, McCulloch J, Teasdale GM (1981) Focal cerebral ischemia in the rat: I. Description of technique and early neuropathological consequences following middle cerebral artery occlusion. *J Cereb Blood Flow Metab* 1:53– 60.

Tortiglione A, Minale M, Pignataro G, Secondo A, Scorziello A, Di Renzo GF, Amoroso S, Caliendo G, Santagada V, Annunziato L (2002) The 2-oxopyrrolidinacetamide piracetam reduces infarct brain volume induced by permanent middle cerebral artery occlusion in male rats. *Neuropharmacology* 43:427– 433.

Trotti D, Rizzini B.L, and Rossi D (1997) Neuronal and glial glutamate transporters possess an SH-based redox regulatory mechanism Eur. J. Neurosci. 9: 1236-1243.

Tsoi M, Rhee KH, Bungard D, Li XF, Lee SL, Auer RN, Lytton J (1998) Molecular cloning of a novel potassium-dependent sodium-calcium exchanger from rat brain. J Biol Chem 273:4155– 4162.

Vogt and Vogt in Adams-Corsellis-Duchen.(eds) (1984) Greenfield's Neuropathology. New York: John Wiley & Sons.

Visser F, Valsecchi V, Annunziato L, Lytton J (2007) Exchangers NCKX2, NCKX3, and NCKX4: identification of Thr-551 as a key residue in defining the apparent K<sup>+</sup> affinity of NCKX2. J Biol Chem 282:4453–4462.

Welch, K. M. A., Caplan, L. R., Reis, D. J., Siesjo, B. K., and Weir, B.(eds) (1997), Primer on Cerebrovascular Diseases. San Diego: Academic Press.

Yaida Y, Nowak TS (1995) Distribution of phosphodiester and phosphorothioate oligodeoxynucleotides in rat brain after intraventricular and intra-hippocampal administration determined by in situ hybridization. Regul Pept 59:193–199.

Zhang YH, Hancox JC (2003) Evidence for a modulatory effect of external potassium ions on ionic current mediated by the cardiac Na<sup>+</sup>/Ca<sup>2+</sup> exchanger. Cell Calcium 33:49 –58.

# ACKNOWLEDGEMENTS

I would like to deeply thank the various people I worked with, during the three years of my PhD experience: first of all there is the Main Chief of the Pharmacology Unit in the Neuroscience Department, Prof. Lucio Annunziato, that was my tutor, and then all the colleagues that contributed to this long work of thesis, Dr. Ornella Cuomo and Dr. Giuseppe Pignataro for the *in vivo* studies, Dr. Francesca Boscia for the *In Situ* Hybridization, Dr. Agnese Secondo for the  $[Ca^{2+}]_i$  measurement, Dr. Anna Pannaccione for the Electrophysiology, Dr. Antonella Scorziello for the cell cultures and the OGD experiments, Dr. Davide Viggiano for the studies on the cerebrovascular anatomy, and Dr. Jonathan Lytton (University of Calgary, Canada) for the Real-Time PCR analysis.